Pergamon

Geochimica et Cosmochimica Acta, Vol. 66, No. 6, pp. 1067–1083, 2002

0016-7037/02 $22.00 + .00

PII S0016-7037(01)00828-6

Spatially correlated anomalous $^{40}Ar/^{39}Ar$ "age" variations in biotites about a lithologic contact near Simplon Pass, Switzerland: A mechanistic explanation for excess Ar

ETHAN F. BAXTER,[1,*,†] DONALD J. DEPAOLO,[1] and PAUL R. RENNE[1,2]

[1]Department of Earth and Planetary Science, University of California, Berkeley, CA 94720, USA
[2]Berkeley Geochronology Center, 2455 Ridge Road, Berkeley, CA 94709, USA

(*Received February* 28, 2001; *accepted in revised form October* 6, 2001)

Abstract—Forty-four biotite samples collected about a lithologic contact between pelite and amphibolite were analyzed for $^{40}Ar/^{39}Ar$ and demonstrate the importance of bulk Ar diffusivity and system geometry—factors not usually considered in the interpretation and collection of $^{40}Ar/^{39}Ar$ age data. The resulting $^{40}Ar/^{39}Ar$ apparent ages range from 11.30 ± 0.05 Ma to 17.90 ± 0.10 Ma. The ages (and excess argon contents) are spatially and lithologically correlated. The pelite samples all yield ages clustering around ~12 Ma, the age expected for cooling through biotite closure (~360°C) in this region of the Alps. Ages in the amphibolite biotites are older, showing a smooth trend between 15 Ma at the contact with the pelite to 18 Ma, 34 cm from the contact. This data shows that characterization of the Ar closure age for biotite in a given system should not rest on a single sample, as otherwise irresolvable differences in age between samples within the same outcrop can exist. A generalized mechanistic model for excess argon is presented. The presence (or absence) of excess Ar depends on an intrinsic system parameter, τ_T, the transmissive timescale, which is the characteristic time for ^{40}Ar to escape through the local intergranular transporting medium (ITM) to some sink for argon. To prevent buildup of geochronologically significant excess ^{40}Ar, τ_T must be very short relative to the true closure age of the mineral. A FORTRAN code including radiogenic Ar production, diffusive loss of Ar from biotite, and bulk Ar diffusion through the ITM has been developed. Application of numerical modeling suggests that the time-averaged effective bulk diffusivity, D_{eff}^{Ar}, in the biotite-amphibolite rock during early retrograde cooling is $2.2 \pm 1.0 \times 10^{-8}$ m^2/yr (assuming steady state conditions) - the first such measurement available. Numerical modeling also provides information about the transmissivity and geologic history specific to the field site, including a drop in D_{eff}^{Ar} at 15.5 ± 1.0 Ma. The timing of this drop is related to coincident rheological changes and the onset of rapid exhumation of the nappe stack. *Copyright © 2002 Elsevier Science Ltd*

1. INTRODUCTION

Interpretations of geochronologic data in the K/Ar system generally assume that there be no non-atmospheric ^{40}Ar within a dated mineral before the time at which it begins to "close" diffusively (Dodson 1973) and in situ produced radiogenic ^{40}Ar begins to accumulate. This assumption is routinely made, unless an "excess Ar" component may be inferred by other means, such as isotope correlation diagrams (Lanphere and Dalrymple, 1971; 1976), or chlorine correlation (Cumbest et al., 1994; Harrison et al., 1994). This assumption, herein referred to as the "zero radiogenic Ar assumption," is apparently widely applicable insofar as ages that are geologically consistent have been measured with the $^{40}Ar/^{39}Ar$ technique in a wide variety of rocks, and the $^{40}Ar/^{39}Ar$ technique has become one of the most used geochronometers.

However, since the inception of the $^{40}Ar/^{39}Ar$ technique, and it's precursor, K/Ar dating, there have been many reports of "excess Ar" in a variety of minerals and geologic environments (see McDougall and Harrison, 1999 and extensive references therein, as well as Kaneoka, 1974; Maluski et al., 1990; Hyodo and York, 1993; Smith et al., 1994; Ruffet et al., 1995; Scaillet, 1996), including biotite, which will be the focus of the present study (e.g., Richards and Pidgeon,1963; Lovering and Richards, 1964; Zartman et al., 1967; Pankhurst et al. 1973; Foland, 1979; 1983; Roddick et al., 1980; Dallmeyer and Rivers, 1983; Phillips and Onstott, 1988, Renne, 1995; Reddy et al., 1996; Pickles et al., 1997; Kelley and Wartho, 2000). "Excess Ar" is defined by McDougall and Harrison (1999) as "that component of ^{40}Ar, apart from atmospheric ^{40}Ar, incorporated into samples by processes other than by in situ radioactive decay of ^{40}K." The presence of excess Ar results in calculated "ages" that are too old, sometimes even older than the age of the Earth (e.g., Pankhurst et al., 1973). Despite its common occurrence, the mechanisms responsible for the presence (or absence) of excess Ar remain poorly understood.

Unless an excess Ar component may be inferred by other means (see above), understanding the occurrence of excess Ar must be considered fundamental to K/Ar and $^{40}Ar/^{39}Ar$ geochronometry. The essential requirement of the zero radiogenic Ar assumption is that radiogenic ^{40}Ar is effectively instantaneously lost from the dated minerals and their immediate surroundings while the dated minerals are still "open." The fact that, in many instances, ^{40}Ar is apparently not so readily lost, suggests that there is a need for quantitative models of Ar transport and partitioning at the local (millimeters) and rock system scale (centimeters to kilometers) to understand not only the conditions under which the zero radiogenic Ar assumption fails, but also the conditions (which may seem at first glance extreme) under which it holds.

* Author to whom correspondence should be addressed (ebaxter@gps.caltech.edu).
† *Present address*: Division of Geological and Planetary Sciences, Caltech, MC 170-25, Pasadena, CA 91125 USA.

This paper presents a model for the origin of excess Ar in metamorphic rocks and applies it to systematic $^{40}Ar/^{39}Ar$ analyses at a field site in the Simplon Alps. Biotites at this site hold variable amounts of excess Ar. Quantitative modeling of the data support a hypothesis that the excess Ar content of a mineral is strongly dependent on the bulk rock Ar diffusivity, and the geometry of the system: factors that are not typically considered in the interpretation of Ar isotopic data. Ultimately, the study is intended to exploit patterns in the existence of excess Ar to provide a more complete understanding of the hydrologic and geochemical transport properties of heterogeneous crustal environments in which Ar is produced and is mobile.

2. PREVIOUS RESEARCH

In general, the common explanation for excess Ar is the presence of a high ambient partial pressure of ^{40}Ar (e.g., Lovering and Richards, 1964; McDougall and Green, 1964; Foland, 1979; Roddick et al., 1980; Harrison and McDougall, 1981; Smith et al., 1994; Scaillet, 1996; Kelley and Wartho, 2000) which requires conditions conducive for the introduction and retention of radiogenic ^{40}Ar within the rock. Roddick et al. (1980) suggested that transient partial pressures and isotopic compositions of ambient Ar, related to the varying ability for atmospheric Ar to penetrate deep in to the crust, could explain the variable amounts of excess ^{40}Ar trapped in some metamorphic minerals. Cumbest et al. (1994) also discussed the extent and timescale for mixing of atmospheric and excess Ar bearing fluids in the crust as a control on ambient Ar isotopic compositions. Foland (1979) showed that variable amounts of excess Ar in biotites in a "relatively anhydrous" charnokite correlate with whole rock potassium content, suggestive of local derivation of excess Ar. Furthermore, Foland (1979) suggests that Ar partial pressures could vary significantly over a scale less than 10 m and consequently Ar transport in the rock must have been restricted. Scaillet (1996) also suggested a model of "internal isotopic buffering" whereby excess ^{40}Ar is locally derived. Low intergranular diffusivities are argued to have promoted centimeter scale variations in argon isotopic content. Kelley and Wartho (2000) measured apparent excess Ar in mantle phlogopites suggesting that these biotites retained Ar at or above 700 °C in the mantle, well above their diffusional closure temperature. They suggest that a lack of Ar exchange with other phases in the system contributes to the excess Ar build up in biotite. Harrison and McDougall (1981) showed that excess Ar released from a degassing gneiss during reheating caused high ambient ^{40}Ar partial pressures which penetrated into neighboring country rock granulites. They found the greatest excess Ar contents preserved in granulite minerals closest to the contact with the gneiss. Others studies show that partial degassing of active magmatic bodies or hydrothermal systems may contribute significant excess Ar (e.g., Burnard et al., 1999). Or, old intrusive or volcanic rocks that may never have fully degassed and equilibrated with atmospheric Ar (e.g., Dalrymple and Moore, 1968) may, upon metamorphism, contain an excess Ar component (e.g., Smith et al., 1994).

3. FIELD SAMPLING AND ANALYSIS

3.1. Field Area

The field site is near Simplon Pass in the Alps of Southern Switzerland (Fig. 1). Sampling was conducted about a sharp, primary lithologic contact between amphibolite and metapelite (Fig. 2). The rocks are structurally situated in the Lebendun Nappe. Protolith deposition was Permian-Carboniferous in age during the waning stages of the Hercynian Orogeny (Bearth, 1972). The rocks experienced peak metamorphic conditions of garnet growth at ~610 °C and ~9 kbars at ~30Ma (Baxter and DePaolo, 2000; Vance and O'Nions, 1992). Slow cooling proceeded at the field site to 540 ± 60 °C at 16.5 ± 1.5 Ma (Fig. 3), at which time the onset of rapid cooling (~40 °C/Ma) commenced (Mancktelow 1992; Grasemann and Mancktelow, 1993) in response to exhumation enhanced by embrittlement (Mancktelow, 1992; Axen et al. 2001), the development of the cataclastic Simplon detachment fault (Mancktelow, 1992) and the passage of a complex rolling hinge through the Simplon footwall (Wawrzyniec et al., 2001). The amphibolite mineralogy is amphibole, garnet, plagioclase, quartz, sphene, ilmenite and apatite ± biotite. There are some carbonate veinlets and chlorite associated with late retrograde processes, but these are of limited extent. Pelite mineralogy includes quartz, plagioclase, biotite, muscovite, and garnet with accessory ilmenite and apatite (see Baxter and DePaolo, 2000; Baxter, 2000 for further details).

The biotite mode in the amphibolite decreases away from the contact to essentially zero beyond ~3 m from the contact. Figure 4 shows the variation of K wt.% with proximity to the contact. The smooth drop in K away from the contact is a strong indication of bulk K diffusion from the K rich pelite into the initially K-poor amphibolite. This trend is disrupted between ~1.4 and 2.3 m from the contact, where the K% (and biotite mode) increase. This zone of anomalously high K wt.% is also characterized by an increase in garnet porphyroblast size and mode, an abundance of layer-parallel quartz veinlets, a few thin lenses of metapelite, galena mineralization in some of the quartz veinlets and anomalously elevated Sr isotope values (Baxter, 2000). This roughly 1 m wide "vein zone" may be traced subparallel to the contact for 10s of meters in either direction where, in one direction, it approaches to within 30cm of the contact before being obscured by colluvium (see Fig. 2). These observations combine to suggest that this was a zone of localized layer subparallel fluid advection, likely expedited by the inhomogeneity of the interlayered pelite lenses (Baxter, 2000).

3.2. Sample Selection and Preparation

Whole rock samples were collected from the pelite and amphibolite along a traverse perpendicular to the contact (Fig. 2). Each whole rock sample weighed between 150 to 300 g and had a dimension of 1.5 to 4 cm in the direction perpendicular to the contact. Samples nearest the contact (97 BSP5 L-S) were continuous. Whole rock samples were coarsely crushed and sieved. Size fractions were examined for the presence of pure biotite grains. The coarsest size fraction containing abundant pure biotite grains was then further worked in a ceramic mortar and pestle and sieved through the same mesh until only pure

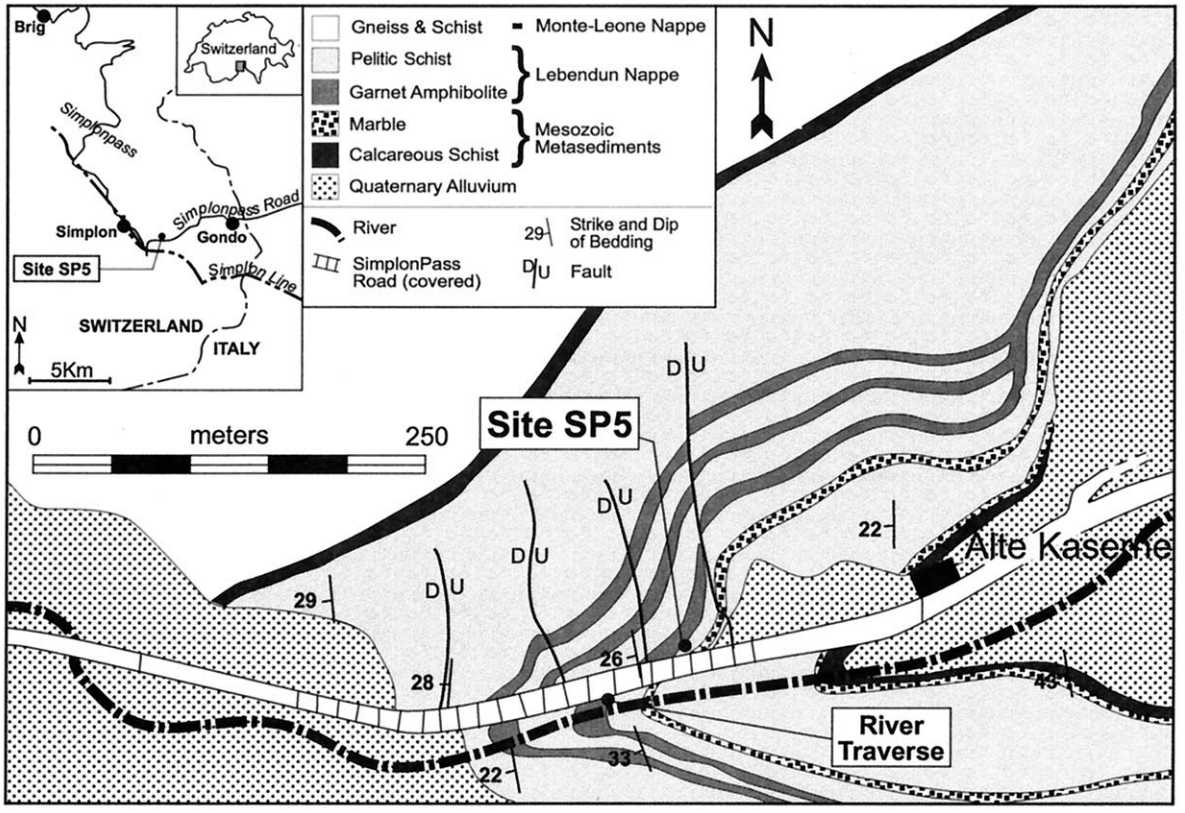

Fig. 1. Geological map of the field site. Taken from mapping by Baxter and DePaolo and the published map of Bearth, 1972. All samples were collected at Site SP5 (see Fig. 2), except samples 98 BSP5 B and 98 BSP5 D which were taken from an outcrop of the same contact in the river just below (river traverse).

biotite flakes remained. Biotite flakes were cleansed in an ultrasonic bath of distilled water and alcohol. Finally, ~10 mg of biotite were handpicked on the basis of their purity and lack of occluded minerals, such as amphibole, plagioclase, or white mica. This procedure results in a separate of pure biotite with grain sizes representative of the largest average natural grain size in the sample (confirmed by thin section). This grain size was 600 to 1000 microns in diameter for all samples except for the two pelite samples closest to the contact (BSP 5-R and BSP 5-S) for which the maximum grain size fraction was 250 to 425 microns in diameter. In addition, two finer grained size fractions of one sample (98BSP 5-Q) were prepared.

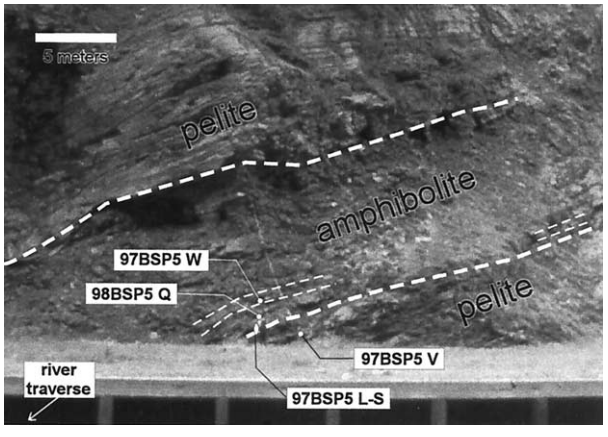

Fig. 2. Photograph of the sampling location, Site SP5, looking NNW. Coarse dashed lines show the approximate position of the pelite-amphibolite contacts. Fine dashed lines show the approximate position of the "vein zone" where exposed. The vein zone is closest to the contact in the rightmost exposure suggesting a layer subparallel trend. The vein zone is also exposed in the river traverse below and to the left where it is even further away from the contact.

Each 10 mg biotite sample was loaded into an aluminum disk along with multiple Fish Canyon sanidine standards (age = 28.02 ± 0.16 Ma) for irradiation (see Renne et al., 1998 for details). After irradiation, four single grains from each sample were analyzed by laser step-heating for $^{40}Ar/^{39}Ar$. Finer grained samples BSP 5-R, BSP 5-S and 98BSP 5-Q were loaded into annealed copper packages and irradiated. After irradiation, these samples were analyzed by stepwise resistance furnace heating for $^{40}Ar/^{39}Ar$. Details of analytical methods are as enumerated in Renne (1995).

3.3. $^{40}Ar/^{39}Ar$ Age Results

The results of the $^{40}Ar/^{39}Ar$ analysis are presented in Table 1 and Figure 5. Four representative age spectra from the pelite and the amphibolite, are shown in Figure 6 a–d. Almost all of the age spectra are very flat and steps consist dominantly of radiogenic ^{40}Ar. Because some of the samples showed discordant apparent ages for initial steps (e.g., Fig. 6a,b), perhaps

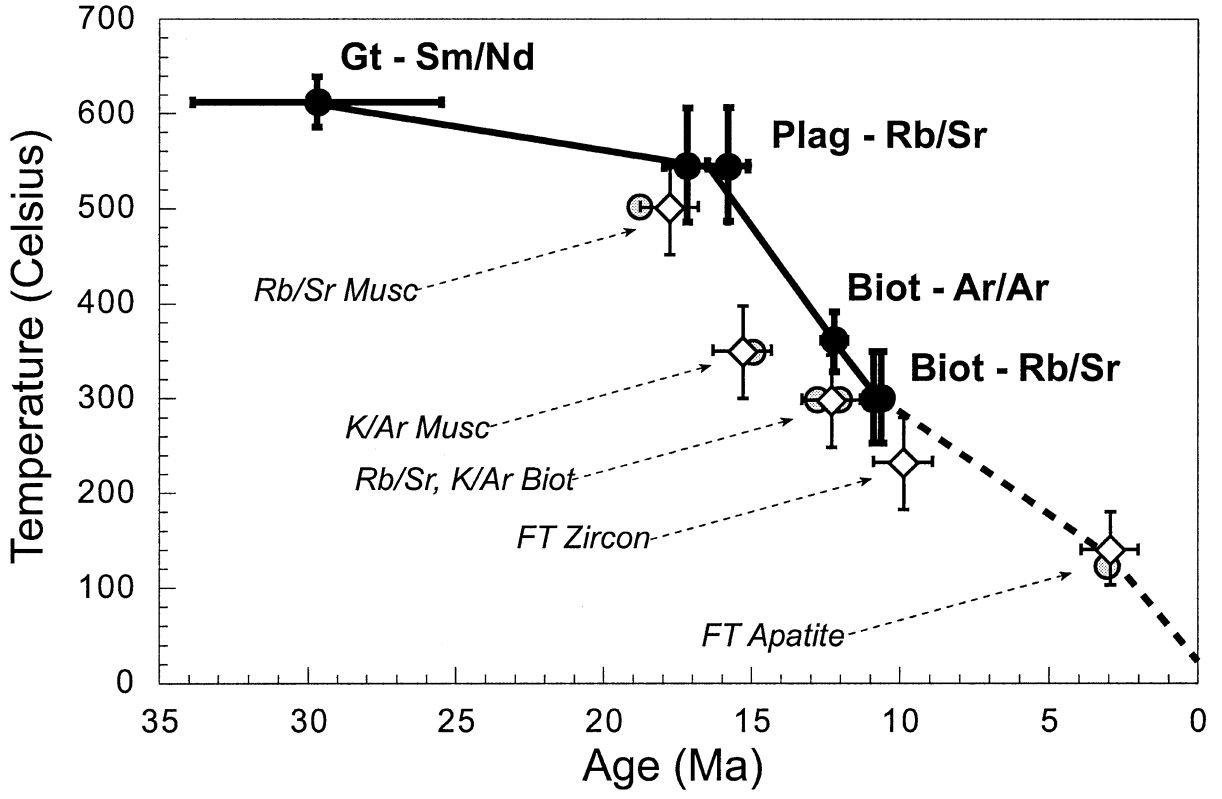

Fig. 3. Thermal history of the rocks at field site SP5. The thermal history used in the model (solid and dashed line) is constrained by T-t data gathered from the outcrop under study. The dashed portion indicates reliance on thermal data not from the field site. Black dots are data obtained from the field site. "Gt Sm/Nd" indicates the temperature and timing of peak garnet growth determined by multi-equilibria geothermometry (Baxter and DePaolo 2000) and a range of available Sm/Nd garnet ages from the area (Vance and O'Nions 1992). Peak temperature error bars are arbitrarily set at ±30 °C, a conservative uncertainty for multi-equilibria geothermometry. "Plag Rb/Sr" indicates plagioclase-whole rock isochron ages reported in Baxter and DePaolo (2000) (with corrected 2σ errors shown). Plagioclase closure temperature is calculated for a 100 μm radius plagioclase sphere using the diffusion data of Cherniak and Watson (1994). "Biot Ar/Ar" indicates the average age and closure temperature measured in the pelite biotites of the current study (see text). Error bars for Biot Ar/Ar and Plag Rb/Sr closure temperatures include uncertainties in grain size and published diffusion parameters. "Biot Rb/Sr" indicate biotite-whole rock isochron ages calculated from data reported in Baxter (2000). In the absence of applicable Sr diffusion data on biotite, Biot Rb/Sr closure temperature is set at the "nominal" 300 °C, and assigned arbitrary ±50 °C error bars. Mancktelow (1992) (gray circles) and Steck and Hunziker (1994) (white diamonds) report thermal data from nearby localities (locality "e" and "Gondo" from those papers, respectively) which is generally consistent with our data from site SP5. While we calculated the closure temperature for minerals using diffusion theory when possible (see above), past workers have simply assigned "nominal" representative mineral closure temperatures. This explains some of the minor differences between our closure temperatures and those reported by past workers. Furthermore, Mancktelow (1992) has shown that thermal histories can vary significantly within a few kilometers of the Simplon Line, so only data collected from site SP5 was used in the model T-t history.

indicative of low temperature weathering effects or preferential release of ^{39}Ar from recoil-damaged near-surface sites, we determined plateau ages for each sample using the criteria defined by Fleck et al. (1977) to remove this minor possible bias from the metamorphic cooling age. Plateau ages are very similar to the integrated ages (see Table 1), hence no significant difference results from using one or the other as the best representation of the biotites' "age." 93% of the samples produced satisfactory plateaus using the above criteria. The ages do not correlate positively with whole-rock K wt.%, contrary to the observation in the study by Foland (1979), but they do correlate strongly with lithology and location (Fig. 5).

The pattern of the data provide two key observations. First, the $^{40}Ar/^{39}Ar$ plateau ages of all pelite samples average 12.2 ± 0.4 Ma (2σ) with no significant variation with proximity to contact. This age, 12.2 Ma, is consistent with published data on the cooling history through biotite closure for both Ar and Sr in this region of the Alps (e.g., Mancktelow, 1992; Steck and Hunziker, 1994; see Fig. 3. The slightly younger ages of samples BSP 5-R and BSP 5-S may be explained by their smaller natural grain size (if grain diameter equals effective diffusional dimension). The second observation is that the biotite ages recorded in the amphibolite are significantly older, and increase from 15.0 Ma at the contact to a maximum of 17.9 Ma at 34 cm and then drop back down to 14.4 Ma at the vein zone. These ages are too old for cooling through biotite closure to be consistent with published cooling data (e.g., Mancktelow, 1992; Steck and Hunziker, 1994; Baxter and DePaolo, 2000)

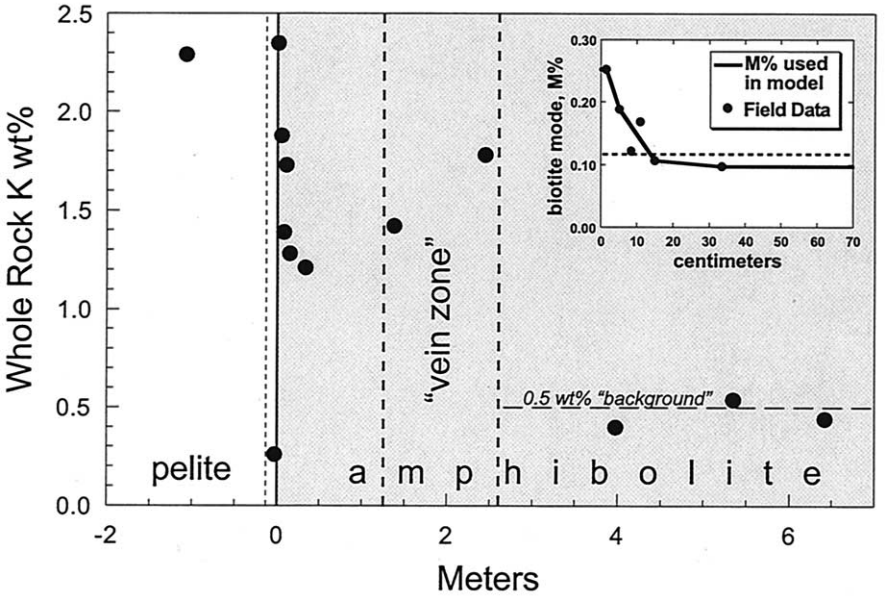

Fig. 4. Plot of whole rock K wt.% in the outcrop. The inset shows the biotite mode (M%) used in the modeling. The dotted line in the inset shows the average M% over that distance. Biotite mode data in the amphibolite was calculated from K wt.% field data by assuming all potassium, above a background value of 0.5 wt.%, was located in biotite. Samples with K wt.% ~0.5 have no biotite—the potassium is located in hornblende. The low point just across the contact into the pelite is in a thin, ~4cm, gradational layer (indicated by the dotted line) of highly siliceous (86 wt.% SiO_2) psammite with some biotite and only trace amphibole.

(see Fig. 3). This age discrepancy in biotites from the same outcrop only centimeters apart is significant far outside of analytical uncertainty.

4. DISCUSSION OF FIELD DATA

There is no information that can be gained from the plateau-shaped biotite age spectra to constrain the presence, absence or amount of excess Ar, in part because biotites may decompose upon heating, destroying and obscuring internal variations in Ar isotopic content (e.g., Hodges and Bowring, 1995; McDougall and Harrison; 1999) that may have revealed an excess Ar component. Thus, excess Ar cannot be distinguished without a priori knowledge of the "true" age. Accepting ~12 Ma as the "true" biotite closure age for the field site, a logical interpretation would be that the biotites located in the amphibolite contain significant excess Ar, whereas those located in the pelite do not. In any case, regardless of the true age, the ca. 50% variation in biotite ages challenge conventional interpretation.

4.1. Assessment of Possible Factors Causing Different Apparent Ages

Before proceeding with this interpretation, let us consider other factors that might contribute to the differing ages observed. The diffusional closure equation (Dodson 1973) gives the closure temperature for a mineral given cooling rate (dT/dt), effective diffusion radius (a), and the intrinsic diffusion parameters for the mineral, D_0 and Q, as:

$$T_c = \frac{Q/R}{\ln\left(\frac{ART_c^2\,(D_0/a^2)}{Q(dT/dt)}\right)} \quad (1)$$

where R is the gas constant, and A is geometric factor. Setting a=400 μm, the median natural radius of analyzed samples[1], dT/dt=40 °C/Ma (see Fig. 3), D_0=0.075 cm^2/s and Q=47.1 kcal/mol (Grove and Harrison 1996), and A=27 (for cylindrical diffusion appropriate for mica, e.g., Onstott et al., 1991; Hames and Bowring, 1994), Eqn. 1 gives a closure temperature of 362 °C.

Let us consider the effect of varying, 1) dT/dt, 2) a, 3) biotite composition, and 4) contamination by older minerals. First, it is untenable that samples only centimeters apart could experience cooling histories different enough (about a factor of five) to account for the variations in biotite age between the pelite and amphibolite. Second, all biotite separates were sieved to the same natural grain size range (see above). The difference in closure temperature between a grain of 300 μm and 500 μm radius is only 16 °C (369 to 353 °C), which would provide just a 0.4 Ma difference in age. This is enough to explain some of

[1] Some uncertainties exist regarding the effective diffusional radius (a) in biotite. Harrison et al. (1985) advocate a ~150 μm effective radius, while Grove and Harrison (1996) and Harrison and McDougall (1999) caution that biotites may in fact have multiple diffusion domains of varying diffussional radii up to the natural grain size. Goodwin and Renne (1991), Onstott et al. (1991), Hess et al. (1993) and Hodges et al. (1994) advocate use of the natural grain size. For simplicity, we have chosen to use the natural grain size. For the purposes of comparison in this paper, the effective diffusional radius used makes no difference so long as it is consistent for biotites of similar natural grain size, which seems likely (see text).

Table 1. Biotite $^{40}Ar/^{39}Ar$ Data.

Meters from contact	Sample name	Analysis	Biotite plateau Ar/Ar age (Ma)[1]	±	Biotite integrated Ar/Ar Age (Ma)	±	$^{40}Ar^*$ (mol/g) calculated[2]	K/Ca atomic ratio[3]	Grain diameter (microns)
−4.72	98 BSP5 B	laser - 01	12.10	0.10	12.03	0.13	1.69E-10	10000	600–1000
−4.72	98 BSP5 B	laser - 02	11.30	0.05	11.26	0.06	1.58E-10	500	600–1000
−4.72	98 BSP5 B	laser - 03	na	na	12.64	0.14	1.77E-10	2300	600–1000
−4.72	98 BSP5 B	laser - 04	12.51	0.09	12.52	0.07	1.75E-10	10000	600–1000
−1.07	97 BSP5 V	laser - 01	11.99	0.06	12.19	0.08	1.68E-10	110	600–1000
−1.07	97 BSP5 V	laser - 02	12.49	0.05	12.67	0.05	1.75E-10	1300	600–1000
−1.07	97 BSP5 V	laser - 03	12.69	0.06	12.73	0.06	1.78E-10	4400	600–1000
−1.07	97 BSP5 V	laser - 04	12.12	0.06	12.25	0.06	1.70E-10	370	600–1000
−0.15	98 BSP5 D	laser - 01	12.34	0.06	12.34	0.06	1.73E-10	980	600–1000
−0.15	98 BSP5 D	laser - 02	12.03	0.07	12.20	0.06	1.68E-10	460	600–1000
−0.15	98 BSP5 D	laser - 03	12.02	0.06	11.94	0.06	1.68E-10	630	600–1000
−0.15	98 BSP5 D	laser - 04	12.77	0.09	12.70	0.07	1.79E-10	10000	600–1000
−0.04	97 BSP5 S	furnace	11.68	0.03	11.56	0.06	1.63E-10	na	250–425
−0.03	97 BSP5 R	furnace	11.77	0.04	11.69	0.04	1.65E-10	na	250–425
0.02	97 BSP5 Q	laser - 01	15.05	0.07	15.11	0.09	2.11E-10	15	600–1000
0.02	97 BSP5 Q	laser - 02	15.60	0.03	15.58	0.03	2.18E-10	73	600–1000
0.02	97 BSP5 Q	laser - 03	15.04	0.04	15.04	0.05	2.11E-10	30	600–1000
0.02	97 BSP5 Q	laser - 04	15.56	0.04	15.61	0.05	2.18E-10	250	600–1000
0.05	97 BSP5 P	laser - 01	15.93	0.08	15.89	0.13	2.23E-10	520	600–1000
0.05	97 BSP5 P	laser - 02	15.37	0.13	15.49	0.14	2.15E-10	260	600–1000
0.05	97 BSP5 P	laser - 03	15.48	0.06	15.42	0.07	2.17E-10	82	600–1000
0.05	97 BSP5 P	laser - 04	15.50	0.10	15.40	0.12	2.17E-10	36	600–1000
0.08	97 BSP5 N	laser - 01	16.32	0.08	16.19	0.11	2.29E-10	260	600–1000
0.08	97 BSP5 N	laser - 02	16.62	0.08	16.30	0.08	2.33E-10	110	600–1000
0.08	97 BSP5 N	laser - 03	16.21	0.05	16.41	0.05	2.27E-10	150	600–1000
0.08	97 BSP5 N	laser - 04	15.77	0.14	15.71	0.15	2.21E-10	150	600–1000
0.11	97 BSP5 M	laser - 01	16.10	0.17	15.39	0.16	2.26E-10	150	600–1000
0.11	97 BSP5 M	laser - 02	16.43	0.06	16.50	0.07	2.30E-10	190	600–1000
0.11	97 BSP5 M	laser - 03	17.30	0.05	17.40	0.05	2.42E-10	65	600–1000
0.11	97 BSP5 M	laser - 04	na	na	14.47	0.11	2.03E-10	80	600–1000
0.15	97 BSP5 L	laser - 01	16.21	0.03	16.28	0.04	2.27E-10	41	600–1000
0.15	97 BSP5 L	laser - 02	16.58	0.03	16.56	0.04	2.32E-10	15	600–1000
0.15	97 BSP5 L	laser - 03	16.58	0.11	16.68	0.12	2.32E-10	81	600–1000
0.15	97 BSP5 L	laser - 04	16.62	0.09	16.58	0.08	2.33E-10	14	600–1000
0.34	98 BSP5 Q	laser - 01	17.83	0.05	17.80	0.05	2.50E-10	19	600–1000
0.34	98 BSP5 Q	laser - 02	17.90	0.10	17.84	0.13	2.51E-10	84	600–1000
0.34	98 BSP5 Q	laser - 03	na	na	21.90	0.30	3.07E-10	6	600–1000
0.34	98 BSP5 Q	laser - 04	16.72	0.11	16.73	0.13	2.34E-10	870	600–1000
0.34	98 BSP5 Q	furnace	17.54	0.03	17.42	0.03	2.46E-10	na	250–425
0.34	98 BSP5 Q	furnace	17.47	0.02	17.25	0.02	2.45E-10	na	425–600
1.38	97 BSP5 W	laser - 01	14.40	0.30	12.70	0.40	2.02E-10	15	600–1000
1.38	97 BSP5 W	laser - 02	na	na	na	na	na	na	600–1000
1.38	97 BSP5 W	laser - 03	14.40	0.13	14.43	0.14	2.02E-10	10000	600–1000
1.38	97 BSP5 W	laser - 04	14.66	0.15	14.26	0.15	2.05E-10	130	600–1000

1-Plateau ages determined as explained in text. na denotes either that no plateau was achieved or that the sample did not run.
2-$^{40}Ar^*$ concentrations were calculated from the age for a biotite ^{40}K concentration of 2.4E-7 (moles ^{40}K/gram biotite).
3-K/Ca atomic ratios are determined from direct measurement of $^{37}Ar/^{40}Ar$ ratios. "10000" was reported when Ca content was below detection limit.

the grain to grain intrasample variations seen, but not the 5.6 Ma variations across the contact. While it is possible that the effective diffusional radius (a) in biotites is as small as 150 μm (e.g., Harrison et al., 1985), it is unlikely that the amphibolite biotites could have had an effective diffusional lengthscale significantly greater than biotites in the pelite. Third, data on the effect of biotite composition on Ar diffusivity (Giletti, 1974; Harrison et al., 1985; Grove, 1993; Grove and Harrison, 1996), suggests that there is a small effect. Three compositional parameters have an important impact on diffusivities, and hence, closure temperatures and ages. The three parameters, Fe/(Fe+Mg), xAl(VI), and F/(F+OH) were measured using the electron microprobe on biotites from representative thin sections at several sample locations (see Table 4). The differences in these compositional parameters between the pelite and amphibolite biotites are minimal, and would only effect net differences of a few degrees in the closure temperature (Grove, 1993; McDougall and Harrison, 1999). Finally, contamination by older occluded hornblende, would produce older ages. We can assess this effect by comparing K/Ca ratios of the measured samples by means of reactor produced ^{37}Ar, and K/Ca ratios measured on pure biotite and hornblende grains with the electron microprobe (Tables 1 and 2). Assuming the hornblende age to be ~29 Ma (Deutsch and Steiger, 1985) we find that possible levels of contamination will have no effect on the measured age (see Fig. 7).

Having rejected other possible causes for variations in the measured ages across the contact, we are left with the interpre-

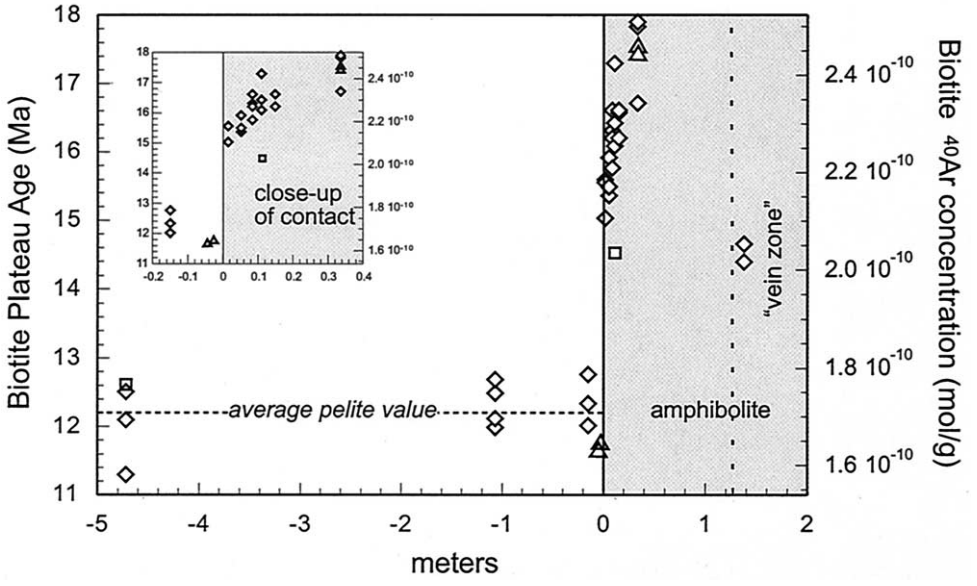

Fig. 5. Plot of biotite $^{40}Ar/^{39}Ar$ age data for biotites at site SP5. Data are shown both as ages (left axis) and as ^{40}Ar concentrations (right axis) calculated from the age on the basis of 2.4×10^{-7} moles ^{40}K/g of biotite. Diamonds denote plateau ages determined from laser step heated single grain samples. Triangles denote plateau ages from finer grained multi-grain furnace step heated samples. Squares denote total integrated ages for single grain samples which did not produce satisfactory plateaus. Sample 98 BSP5-Q laser-03 (21.90 Ma) is off scale.

tation that varying amounts of excess ^{40}Ar remained in the biotites within the amphibolite. Pelite biotites, on the other hand, appear to have satisfied the "zero radiogenic Ar assumption" as they yield consistent and geologically expected ages. The smooth pattern of ages in the amphibolite further suggests a correlation between proximity to the pelite-amphibolite contact and the amount of excess Ar, with the greatest excess Ar furthest from the contact. Biotites from the "vein zone" also exhibit less excess Ar than elsewhere in the amphibolite.

4.2. Model Hypothesis for Excess Ar

4.2.1. Requirements for the "zero radiogenic Ar assumption"

To develop a mechanistic explanation for the spatially correlated biotites ages at the field site, let us first step back and examine the general conditions required to satisfy the "zero radiogenic Ar assumption" and prevent excess Ar. Consider a K-bearing source mineral within a metamorphic rock at depth that is producing ^{40}Ar well above its closure temperature (Fig. 8). As ^{40}Ar is produced within the K-bearing mineral, ^{40}Ar may freely diffuse out of (or into) that mineral and into the local intergranular transporting medium (ITM) which surrounds it. The ITM is the network of grain boundaries, whatever their characteristics (i.e., wetted or dry), which is the medium through which chemical transport is most rapid in rocks (e.g., Brady, 1983; Farver and Yund, 1995; Baxter and DePaolo, 2000). Despite its *ability* to do so, whether or not ^{40}Ar will thermodynamically favor continuous and complete diffusion out of the source mineral depends on the capacity for the local ITM to take in ^{40}Ar and transmit it, ultimately, to some sink for Ar. Stated differently, the question is whether or not the surrounding ITM behaves as an *effective* zero concentration boundary condition for radiogenic ^{40}Ar diffusing out of the source mineral. Let us assume that the equilibrium source-mineral/ITM partition coefficient (K_d) for Ar is non-zero, though it may be a very small number (e.g., Roselieb et al., 1997; Brooker et al., 1998; S.P. Kelley private communication). The local ITM, which comprises only a tiny volume fraction (i.e., porosity, ϕ) of the rock, cannot itself behave as an effective sink for Ar unless the product MK_d is much less than 1 (M is defined here as the mass ratio of source mineral (biotite) to ITM; see Table 3 for details). To satisfy the zero radiogenic Ar assumption, ^{40}Ar must not accumulate in the local ITM, or there will be a proportional (by K_d) buildup of excess ^{40}Ar in the source mineral.

4.2.2. Importance of the transmissive timescale

To prevent *any* buildup of excess ^{40}Ar in the K-bearing source mineral, the ITM must behave as an infinitely transmissive medium such that ^{40}Ar introduced into the ITM from local K-bearing mineral sources is efficiently and immediately removed from the system to some sink for Ar. The transmissivity may be advective (V*=total effective velocity) or diffusive (D*=total effective diffusivity, defined in Section 5.1). We define a parameter, the transmissive timescale, τ_T as:

$$\tau_T = \tau_D = \frac{L^2}{D^*} \text{ for diffusive transport, and}$$

$$\tau_T = \tau_A = \frac{L}{V^*} \text{ for advective transport}$$

If, for the sake of argument, we assume that the Ar sink is located a distance, L, away from the local source, the general requirement is that τ_T must be very short relative to the timescale of local ^{40}Ar radiogenic production. τ_T is the character-

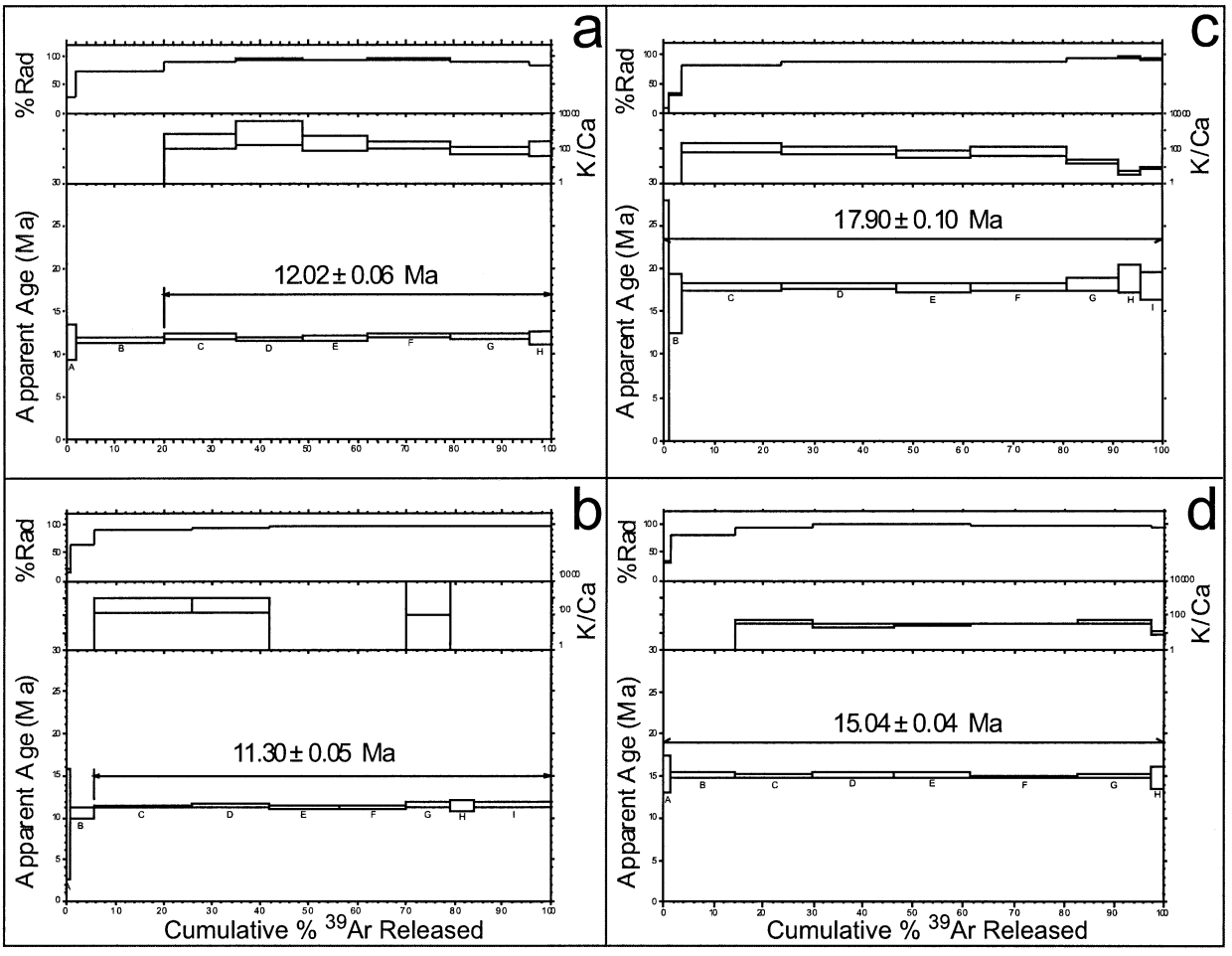

Fig. 6. Representative age spectra for pelite (a,b) and amphibolite (c,d) biotites.

istic time for ^{40}Ar to escape through the local ITM to a sink for argon. Therefore, for geochronological purposes, the excess ^{40}Ar in the mineral is negligible for sufficiently small τ_T, (τ_T less than ~0.1% of the true age). For older minerals, the requirement of "infinite transmissivity" is relaxed—some amount of excess ^{40}Ar may be permitted, but would be dwarfed by the amount of ^{40}Ar*.

The sink for Ar is ultimately the atmosphere itself, which would imply L >10 km for midcrustal environments. However, *effective* sinks may be present at the meso- or micro- scale as shear zones or rock units with very rapid transmissivity or possibly as local non K-bearing mineral sinks, in which case L could be on the scale of millimeters. We will return to the issue of effective Ar sinks later.

The model suggests that portions of the crust with longer characteristic τ_T should accumulate more excess ^{40}Ar (Fig. 9). In such systems, there will be a characteristic buildup of excess ^{40}Ar (at steady state) in the minerals and surrounding ITM proportional to τ_T. In general, the excess "age," caused by excess ^{40}Ar retained in the local ITM at steady state, is of order τ_T. In detail, the amount of steady state excess ^{40}Ar buildup depends also on the geometry of the system, the variability of ^{40}Ar production (i.e., potassium content), and the flux of ^{40}Ar into the local ITM from other sources, local or distal. This conceptual model is broadly similar to the explanations for excess Ar suggested by Foland (1979), Scaillet (1996), and Kelly and Wartho (2000).

4.2.3. Applying the model hypothesis to the field data

Returning now to the field data, the patterns of excess Ar in biotite could be best explained if the limiting factor in the escape of ^{40}Ar from the amphibolite biotites was the rate at which Ar can diffuse *through the amphibolite ITM* into the pelite. Another possibility, cross-layer advection of excess ^{40}Ar from the pelite, cannot explain the fact that the highest excess Ar is far from the contact. Also, Sr isotopic data suggest that cross-layer advection was not important at the field site (Baxter and DePaolo, 2000). In the diffusional escape model, once the ^{40}Ar reaches the pelite, it is then able to escape rapidly to an Ar sink from there. In this way, we can visualize the pelite (and the vein zone of fluid advection at 1.4 m) as effective sinks for Ar *relative to the amphibolite*, at least insofar as they must be characterized by much shorter τ_T (i.e., little excess ^{40}Ar). The amount and pattern of ^{40}Ar buildup in the biotites of the amphibolite will therefore depend on the total bulk diffusivity

Table 2. Electron Microprobe Analyses of Biotites.

Sample name	97 BSP V	97 BSP R	97 BSP Q	97 BSP P	97 BSP N	97 BSP M	97 BSP L	97 BSP W
Meters	−1.07	−0.03	0.02	0.05	0.08	0.11	0.15	1.38
SiO_2	35.68	38.19	36.82	36.95	36.43	36.94	36.67	35.16
TiO_2	1.74	2.12	1.87	1.91	1.89	1.92	1.80	2.11
Al_2O_3	18.58	15.36	16.43	16.80	16.13	16.31	16.45	14.90
FeO	19.78	17.77	17.28	16.22	17.52	16.91	17.34	20.54
MnO	0.19	0.13	0.24	0.23	0.48	0.30	0.30	0.14
MgO	9.03	10.31	12.49	12.60	11.86	12.70	12.20	10.61
BaO	0.11	0.02	0.25	0.07	0.11	0.09	0.08	0.16
CaO	0.01	0.08	0.04	0.01	0.05	0.03	0.06	0.11
na_2O	0.10	0.11	0.12	0.14	0.11	0.13	0.12	0.10
K_2O	9.67	6.52	9.51	9.27	9.59	9.62	9.57	8.83
F	0.24	0.26	0.26	0.24	0.22	0.29	0.24	0.43
Cl	0.01	0.01	0.01	0.02	0.01	0.01	0.01	0.04
SrO	0.00	0.00	0.01	0.00	0.01	0.00	0.00	0.03
Oxide Totals	95.15	90.90	95.33	94.50	94.43	95.25	94.83	93.15
xFe/(Fe+Mg)	0.55	0.49	0.44	0.42	0.45	0.43	0.44	0.52
xAl(VI)	0.15	0.13	0.09	0.11	0.09	0.09	0.09	0.06
xF(F+OH)	0.06	0.06	0.06	0.06	0.05	0.07	0.06	0.11
K/Ca	2067	93	273	860	215	377	189	92

1-for each sample the average of 3–10 probe analyses is reported.
2-calculated using the program CMP2.exe available with the TWQ software of Berman 1991.

of Ar in the amphibolite matrix (D*), and the diffusive length-scale, L, of the system (i.e., the half-width of the amphibolite layer between the pelite and "vein zone"). For a relatively constant D*, a steady state may be reached where the flux of ^{40}Ar into the ITM from radiogenic production in the biotites will be matched by the flux of ^{40}Ar out of the amphibolite ITM to the pelite. The steady state profile is characteristic of the system τ_T.

5. NUMERICAL MODELING

5.1. Governing Equations

A FORTRAN code was developed to simulate the model hypothesis and to derive the physical parameters that provide a fit to the field data. Two governing equations are required: one that describes the evolution of ^{40}Ar concentration in the ITM (C_f), and one that describes the evolution of ^{40}Ar concentration

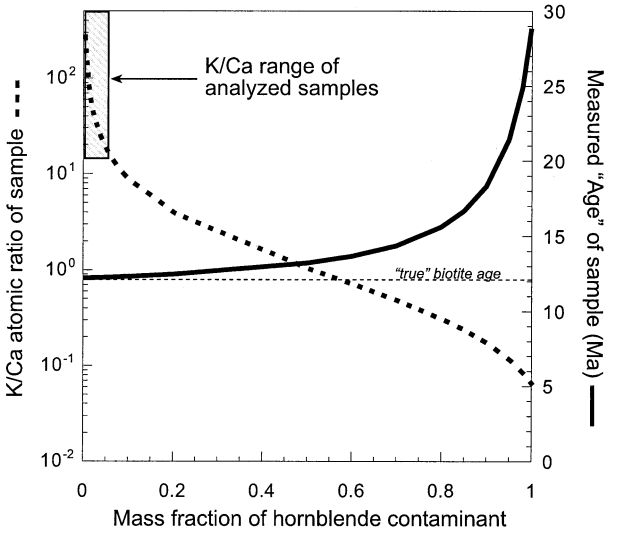

Fig. 7. Plot of the possible effect of amphibole contaminant on biotite ages. Dashed line is the K/Ca ratio of the contaminated biotite/amphibole mixture. Solid line is the resultant measured $^{40}Ar/^{39}Ar$ age of that mixture. Given the range of K/Ca ratios measured on the actual samples from the field site (Table 1), contamination of amphibole could not have exceeded ~6% and therefore would have a negligible effect on age.

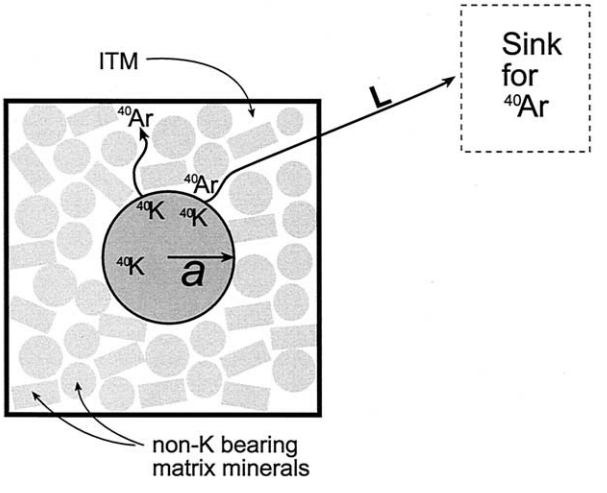

Fig. 8. Conceptual sketch of the production and release of ^{40}Ar. ^{40}K located in a biotite grain (center) decays to produce ^{40}Ar which may then diffuse out into the local ITM. To prevent significant build up of ^{40}Ar in the biotite, the ITM must behave as an efficiently transmissive medium for ^{40}Ar to escape from the local ITM to some sink located a distance "L" away. Note that the ITM volume is greatly exaggerated for illustrative purposes. In reality the porosity is of order 10^{-4}–10^{-5} (e.g., Walther and Wood 1986).

Table 3. Definition of Terms in Equations 2 and 3.

a	4.0×10^{-4} m, radius of average biotite grain (meters)
C_{40K}	2.4×10^{-7} mol/g, specified constant ^{40}K concentration in biotite (moles/gram)
C_f	^{40}Ar concentration in the fluid (moles/gram)
$C_{s(i_{max})}$	^{40}Ar concentration at the outer edge radial increment, i_{max} of biotite grain (moles/gram)
$C_{s(ave)}$	average integrated ^{40}Ar concentration in biotite grain (moles/gram)
D_f	diffusivity of Ar in the ITM with tortuosity correction (meters^2/year)
D_s	radial solid state diffusivity of Ar in biotite (meters^2/year)
i	radial increment index in biotite (0=center, i_{max}=edge)
K_d	equilibrium partition coefficient for Ar between biotite/fluid
M	$\frac{\rho_s M\%}{\rho_f \phi}$, mass ratio of solid to fluid where
M%	mode of biotite (cc/cc), calculated from the whole rock K wt% assuming all potassium above a 0.5% baseline as being housed in the biotite (see figure 4)
r	$i\delta$r, radial position in biotite (meters)
t	time (years)
x	spatial coordinate perpendicular to the layering (meters)
ϕ	Volume fraction of the ITM, i.e. porosity (cc/cc)
λ_{40K}	5.810×10^{-11} yr^{-1}, effective decay constant for ^{40}K decay to ^{40}Ar (years^{-1})
ρ_f	1.0 g/cc, density of intergranular fluid (grams/cc)
δr	arbitrary radial increment in biotite (meters)
ρ_s	3.0 g/cc, density of biotite (grams/cc)

in the solid biotite grains (C_s). These equations are similar in form to those developed by Richter and DePaolo (1987), and used by Johnson and DePaolo (1994) and Baxter and DePaolo (2000) to describe broadly similar systems of ITM mediated transport coupled with ITM-mineral exchange. The key difference for the current application is that local ITM-mineral exchange will be via solid-state diffusion. Transport of ^{40}Ar in the rock matrix will be simplified as one-dimensional, layer perpendicular diffusional transport through the ITM. Diffusion of ^{40}Ar out of the biotite grains will be calculated as radial diffusion out of a cylindrical (or disk-shaped) mineral. The "height" of the model biotite disk will be scaled to account for the variable mode of biotite at each node in the system (see Appendix A, Fig. A1). The other minerals in the amphibolite matrix (mostly amphibole, 60 to 80% and plagioclase, 10 to 20%) will be ignored and treated as inert phases. This simplification is justified because they are not major producers of ^{40}Ar. Furthermore, hornblende Ar closure ages are ~29 to 25 Ma (Deutsch and Steiger, 1985), at a closure temperature well above that of biotite (e.g., McDougall and Harrison, 1999; Harrison, 1981), so hornblende will be an increasingly insignificant source or sink of ^{40}Ar after that time. Few data exist about the closure properties of plagioclase, but it appears that it may remain open to temperatures at or below biotite closure—~200 to 300°C (e.g., Renne 2000). However, preliminary partitioning data suggests that Ar may not partition significantly into plagioclase (S.P. Kelley, private communication.), so we treat it as inert for simplicity. The governing equations are as follows (see Appendix A for derivation and details of numerical expressions; see Table 3 for definition of terms):

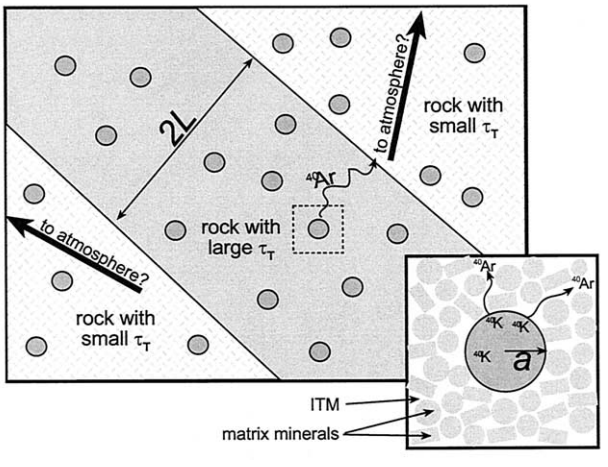

Fig. 9. Conceptual model for limited Ar loss from a more retentive rock layer. The inner layer (shaded) has a slow enough D_{eff} for Ar (i.e., large τ_T) such that ^{40}Ar release to the nearest effective sink (i.e., rocks with short τ_T) is limited by the slow D_{eff} as well as the diffusional lengthscale, L. At the field site, the effective sinks are the pelite and the vein zone surrounding the more retentive amphibolite.

$$\frac{\partial C_f}{\partial t} = D_f \frac{\partial^2 C_f}{\partial x^2} - \frac{2MD_s}{a} \cdot \frac{(K_d C_f - C_{s(i_{max})})}{\delta r} \quad (2)$$

for the fluid ^{40}Ar concentration, and

$$\frac{\partial C_{s(ave)}}{\partial t} = \frac{2D_s}{a} \cdot \frac{(K_d C_f - C_{s(i_{max})})}{\delta r} + \lambda_{40_K} C_{40_K} \quad (3)$$

for the average biotite solid ^{40}Ar concentration.

These two equations are written in a hybrid form between a partial differential equation and a numerical approximation. This is done to illuminate the mathematics of exchange between solid biotite and fluid at the grain edge. The first term in the fluid equation accounts for the flux of ^{40}Ar from each point in the amphibolite towards the pelite sink, and the second term accounts for the flux of ^{40}Ar from the biotite into the ITM, scaled by the solid/fluid mass ratio and the differential form for radial diffusion out of a cylinder. Additionally, we must keep track of the radial C_s profile in the biotite at each X-node in the system to determine $C_{s(imax)}$ and $C_{s(ave)}$. The equation for radial diffusion out of a cylinder for all interior radial increments is:

$$\frac{\partial C_{s(i)}}{\partial t} = D_s \frac{\partial^2 C_s}{\partial r^2} - \frac{D_s}{r} \cdot \frac{\partial C_s}{\partial r} + \lambda_{40_K} C_{40_K} \quad (4)$$

In the numerical approximations, $C_{s(i\max+1)} = K_d C_f$. The equation for $C_{s(ave)}$ may be derived simply by summing cylindrical shells for each radial C_s increment calculated by Eqn. 4.

It is useful to recast Eqn. 2 and (3) in terms of non-dimensional variables. To accomplish this let:

$$C_f' = K_d C_f \qquad x' = x/L \qquad t' = D_f t/L^2 \qquad r' = r/a \tag{5}$$

and, define:

$$D_{eff} = \frac{D_f \phi}{K_d} \qquad D^* = \frac{D_f}{MK_d} = \frac{D_{eff}\rho_f}{M\%\rho_s}$$

$$De = \frac{2D_s L^2}{a^2 D^*} \qquad Dd = \frac{\lambda_{40_K} L^2}{D_f} \tag{6}$$

where L is the diffusional lengthscale of the system. Note the relationship between D_{eff} and D^*, and the fact that it is D^* which determines the transmissive timescale: $\tau_D = L^2/D^*$. Substituting these in and re-arranging yields:

$$\frac{\partial C_f'}{\partial t'} = \frac{\partial^2 C_f'}{\partial x'^2} - De \cdot \frac{(C_f' - C_{s(i_{\max})})}{\delta r'} \tag{7}$$

and

$$\frac{\partial C_{s(ave)}}{\partial t'} = \frac{De}{MK_d} \cdot \frac{(C_f' - C_{s(i_{\max})})}{\partial r'} + Dd C_{40_K} \tag{8}$$

The equations are now similar in form to those derived and solved analytically by DePaolo and Getty (1996). D_e is a type of "Damkohler Number" and may be referred to as a "diffusion exchange" parameter, where in this case, the fluid-mineral exchange is itself mediated by solid state diffusion. D_d is a parameter relating the radioactive timescale to the fluid diffusion timescale. Analogous analytical solutions presented by DePaolo and Getty (1996) indicate that for this system of equations, if L, a, λ, ρ_s, ρ_f, M% and C_{40K} are specified, and MK_d is $>>1$ (i.e., the ITM itself is not an effective sink), the only two adjustable parameters are D_s and D_{eff}. The assumption that $MK_d >> 1$ for the amphibolite is easily justified by the mere fact that the biotites there have excess Ar, so the ITM cannot be acting as a perfect sink. We specify how D_s varies with time during the simulation using a cooling history based on available data (Fig. 3). Uncertainties in the cooling history effect only the closure interval for biotite, and thus have no effect on model results before that time during simulation (i.e., "steady state regime," see below). The arbitrary starting time for simulations was 29.7Ma, about the time of peak metamorphism for which we have a thermal constraint. This starting time makes no difference so long as a steady state is reached during the simulation (see below). Therefore, the only adjustable parameter in the simulations is D_{eff}, including if and when it must vary.

Fixed boundary conditions are imposed at the contact of the amphibolite with the pelite (at x=0) and with the vein zone (at x=140cm):

$$C_f^{(x=0)} = C_f^{(x=140)} = 0 \tag{9}$$

This treats the pelite and vein zone as effective sinks for ^{40}Ar. In the modeling, L = 70cm, the half distance between the pelite and vein zone. For simplicity and speed, the K wt.% profile was treated as symmetric about 70 cm so that only the 0 to 70 cm part of the profile was explicitly modeled. The initial condition is:

$$C_f = C_s = 0, \text{ for all x.} \tag{10}$$

Evolution of ^{40}Ar in the pelite biotites was also explicitly computed using Eqn. 4 in a separate numerical code with a fixed zero concentration boundary condition in the surrounding pelite ITM. Otherwise, the same temperature-time path, grain size, and diffusion parameters were used. This is analogous to the standard model for diffusional closure given the "zero radiogenic Ar assumption" and gives a resulting closure temperature similar to Eqn. 1. The small difference is due to the nonlinear cooling path.

5.2. Numerical Modeling Results

Results of a few representative model simulations for different values of D_{eff} are plotted against the measured ^{40}Ar/^{39}Ar data from the SP5 biotites in Figure 10. The best fit to the data requires a specific D_{eff} history as cooling proceeded. The best fit was achieved for D_{eff} initially equal to $2.2 \pm 1.0 \times 10^{-8}$ m^2/yr, and at 15.5 ± 1.0 Ma, D_{eff} dropping to 1.0×10^{-11} m^2/yr or less (see Fig. 10, 11). The conservative uncertainties reflect the sensitivity of varying each parameter from the modeling as shown in Figure 10. From this result, we define three evolutionary regimes termed "steady state," "transient state," and "closed state." The timing of these three regimes, and the magnitude of D_{eff} therein, controls the final pattern of ^{40}Ar in the biotites. Hence the three key parameters are D_{eff}^{ss}, the initial value of D_{eff} during the "steady state" regime, D_{eff}^{ss}, the value of D_{eff} during the "transient state" regime, and t_{step}, the arbitrary time at which the value of D_{eff} changes. The biotite ^{40}Ar evolution during each of these three regimes is illustrated in Figure 12.

First is the "steady state" regime which lasts from the beginning of simulation until the time, t_{step}, when D_{eff} drops to a lower value. During the "steady state" regime, after ~5 My, the flux of ^{40}Ar out of the biotites into the local ITM becomes equal and opposite to the flux out of the amphibole layer and a steady state ^{40}Ar profile is reached. During this time, Ds remains very fast, as temperatures are well above the closure temperature for biotite. Therefore the biotite (C_s) and ITM (C_f) ^{40}Ar concentrations remain in local equilibrium throughout the "steady state" regime.

The best fit value of D_{eff} during the "steady state" regime, $D_{eff}^{ss} = 2.2 \pm 1.0 \times 10^{-8}$ m^2/yr, is constrained by the slope of the biotite data observed in the amphibolite shown by "Δss" in Figure 10a. The characteristic steady state τ_D of the amphibolite system is 8.0 My (calculated using the average system M% of 0.12, see Fig. 4. Excess ^{40}Ar accumulation in biotites by the end of the steady state regime ranges from 0.0 mol ^{40}Ar/g (or 0.0 My excess age equivalent) for biotite in the pelite or immediately at the contact, to 4.3×10^{-11} mol ^{40}Ar/g (or 3.1 My excess age equivalent) for biotites at L=0.7 m from the contact (see Fig. 12). This excess ^{40}Ar profile is unique for the system τ_D given the boundary conditions *if a steady state was reached*. It is also possible that Δss could be reproduced if τ_D were longer (i.e., smaller D_{eff}^{ss}) and the steady state had not yet been reached. In this scenario, D_{eff} would have to be much

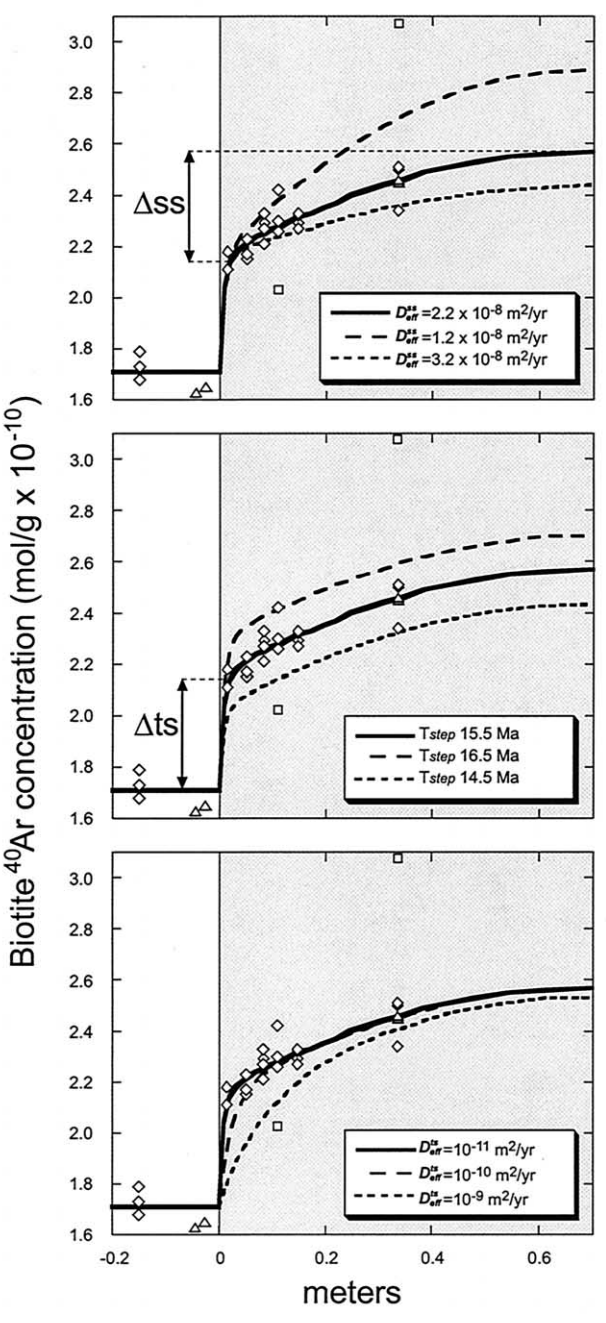

Fig. 10. Plots of model results for a range of parameters illustrating the quality of the fit to the data and constraints on the D_{eff} history. ^{40}Ar* concentrations for the field data are calculated directly from the measured ages for the specified ^{40}K concentration of biotite used in the model ($C_{40K} = 2.4 \times 10^{-7}$ moles ^{40}K/g biotite). A) Effect of changing D^{ss}_{eff} only. B) Effect of changing t_{step} only. C) Effect of changing D^{ts}_{eff} only. For each plot, other parameters are set to the best fit values. Conservative constraints that can be placed on D^{ss}_{eff} and t_{step} are: $D^{ss}_{eff} = 2.2 \pm 1.0 \times 10^{-8} m^2/yr$, and $t_{step} = 15.5 \pm 1.0$ *Ma*, as shown. The subtle kinks in the model results are due to the variations in whole rock K wt.%. Δss and Δts are defined in the text. Data symbols are as defined in Figure 5. Integrated ages for the two samples which did not produce satisfactory plateaus (squares) lie well outside the range of the other data and were not considered in the fit.

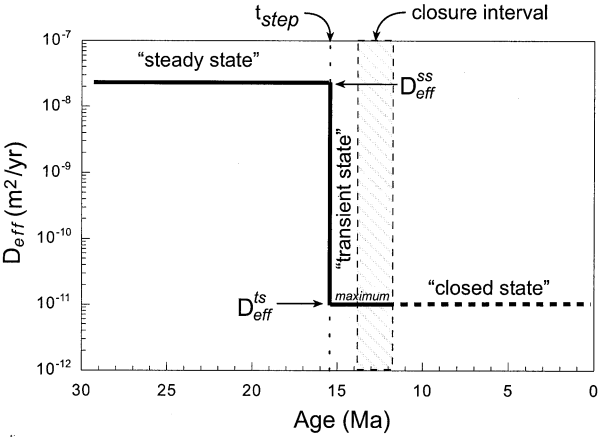

Fig. 11. Evolution of Ar D_{eff} in the amphibolite at site SP5 constrained by the modeling and best fit to the data. The abrupt drop in Ar D_{eff} at 15.5 ± 1.0 Ma was likely a more gradual transition in nature than depicted here.

higher before ~18.6 Ma, preventing earlier ^{40}Ar buildup, or else Δ*ss* (3.1 Ma) would not be reproduced. However, modeling of Sr isotope data from the field site (Baxter and DePaolo 2000) suggests that bulk chemical diffusivities *increased* from at least 29.7 ± 4.2 Ma until 16.5 ± 1.5 Ma (see Section 5.3.1). Thus, we assume that a steady state was reached, and the best fit D^{ss}_{eff} (and τ_D) from the modeling represent values appropriate for the period of early retrograde cooling under study. As we have no way of constraining possible short period fluctuations in D_{eff} during the "steady state regime," the D^{ss}_{eff} constrained by the model represents the *time-averaged* D_{eff} characterizing the system over that period of time.

The "transient state" regime lasts from the time, t_{step}, until the diffusional closure time for biotite, 12.2 Ma, the age recorded by the pelite biotites not subject to the accumulation of excess Ar. D_{eff} must drop during the "transient state" regime to reproduce the observed step in ^{40}Ar content between pelite biotites and amphibolite biotite immediately across the contact,

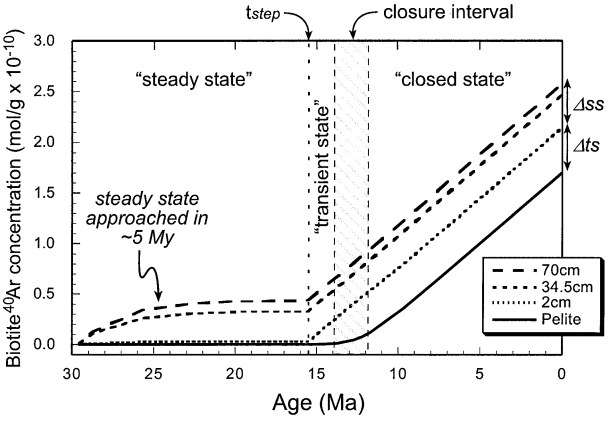

Fig. 12. Temporal evolution of ^{40}Ar concentration in biotites at different proximities to the pelite-amphibolite contact at the field site. The lines are for biotite in the amphibolite located 2, 34.5, and 70 cm from the contact, and for a biotite in the pelite. Note the buildup to the steady state concentration profile during the steady state regime.

denoted by Δts in Figures 10b and 11. The timing of the drop, $t_{step} = 15.5 \pm 1.0$ Ma, is well constrained by Δts (see Fig. 10b) and D^{ts}_{eff} must be 10^{-11} m^2/yr or less (see Fig. 10c). This drop essentially closes the entire amphibolite rock to further escape of ^{40}Ar. So, even though all the biotites in the system remain above their closure temperatures during this time interval, since the amphibolite D_{eff} is so low, the ^{40}Ar produced from the biotites cannot get out of the amphibolite matrix itself to the pelite and the Ar sink. This drop in D_{eff} is unique to the particular fluid-rock and tectonic history of the field site.

The "closed regime" begins after the diffusional closure interval when radiogenic ^{40}Ar begins to accumulate quantitatively in all biotites (of the same diffusional radius) until the present.

5.3. Discussion of Model Results

5.3.1. Comparison to Sr bulk diffusivity

The results of the model simulations show that the conceptual model can explain the observed data quite well and provides us with an estimate for the effective diffusivity of Ar in the biotite-amphibolite during early retrograde cooling: $2.2 \pm 1.0 \times 10^{-8}$ m^2/yr. Independent modeling of Sr isotopic data from the field site (Baxter and DePaolo, 2000) suggest that the D^* for Sr is the same in both the pelite and amphibolite-increasing from 2×10^{-9} (at 29.7 ± 4.2 Ma) to 2×10^{-7} m^2/yr (at 16.5 ± 1.5 Ma). Since all mobile elements share the same ITM, we might infer that D^{ss}_{eff} for Ar in the pelite should also be the same as in the amphibolite ($2.2 \pm 1.0 \times 10^{-8}$ m^2/yr). Or, Ar D^{ss}_{eff} could be different in the pelite if K^{Ar}_d varies between the bulk pelite and bulk amphibolite, which is possible (see below). The observation that both Ar and Sr D^{ss}_{eff} in the amphibolite are similar is interesting in and of itself.

5.3.2. Significance of the 15.5 ± 1.0 Ma drop in D_{eff}

The timing of the drop in amphibolite D_{eff} ($t_{step} = 15.5 \pm 1.0$ Ma), constrained by the modeling presented above, coincides closely with the onset of rapid exhumation at ~16 Ma (Mancktelow, 1992; Grasemann and Mancktelow, 1993; Steck and Hunziker, 1994; Fig. 3) which was promoted by significant rheological and tectonic changes (Mancktelow, 1992; Wawrzyniec et al. 1999; Axen et al. 2001; Wawrzyniec et al., 2001). Mancktelow (1992) shows that the area passed through the ductile-brittle transition at ~16 Ma, and that the Simplon detachment fault first developed at the same time. Grasemann and Mancktelow (1993) show that the most rapid exhumation occurred within 18 to 15 Ma. Wawrzyniec et al. (1999) and Axen et al. (2001) also show that the rocks at the field site underwent permanent "embrittlement" at the same time which contributed to the onset of micro- to macro-scale faults and associated fracturing. Furthermore, the pelite appears to have been much more susceptible to "embrittlement" than the amphibolite, creating a significant rheological difference between the pelite (semibrittle) and the amphibolite (ductile) after 16 Ma (T. F. Wawrzyniec, private communication). Finally, these rheological changes promoted (or enhanced) the passage of a complex rolling hinge through the area of study allowing for the onset of rapid exhumation along these structures (Wawrzyniec et al., 2001). These structural and rheological changes all at ~16 Ma are unlikely to be coincidence, and probably relate mechanistically to the drop in amphibolite D_{eff} that we have *independently* inferred at the same time. Changes in the porosity or redistribution of fluid between highly fractured pelite and unfractured amphibolite, changes in fluid composition (i.e., more carbonitic and less wetting, Wawrzyniec et al. 1999), or strain induced reorganization of the amphibolite ITM associated with the above changes could all explain the drop in amphibolite D_{eff} at 15.5 ± 1.0 Ma.

5.3.3. Different behavior of argon in pelite vs. amphibolite before 15.5 ± 1 Ma

While there is much reason to suspect that the pelite and amphibolite behaved fundamentally differently after the changes that occurred at ~16 Ma (see above), there is no evidence for such a difference before 16 Ma. In fact, the Sr isotopic data (Baxter and DePaolo, 2000) suggest that there were no apparent differences in the layer-perpendicular bulk transport characteristics of the pelite and amphibolite previous to 16 Ma (during the steady state regime). Therefore, it is difficult to reconcile how τ_T in the pelite could have been so short in comparison to the amphibolite- so as to prevent excess Ar build-up as observed. There are two ways to decrease τ_T: 1) by increasing D_{eff} (or V_{eff}), or 2) by decreasing L. We consider these possibilities below.

If the final sink for Ar were the atmosphere, then the effective transmissive lengthscales, L, would be 70 cm for the amphibolite vs. >10 km for the pelite during the "steady state regime." Given these L values, in order for τ_T to be much shorter in the pelite than in the amphibolite, $D^*_{pelite} >> D^*_{amph} \cdot 2 \times 10^8$ for diffusive transport, or $V^*_{pelite} >> V^*_{amph} \cdot 1.44 \times 10^4$ for advective transport. This is an extremely large difference to account for. D* (or V*) for Ar within the pelite could be higher than in the amphibolite if, 1) more brittle pelite rheology and abundant fractures created rapid pathways for migration; 2) the pelite $MK_d << 1$ due to a greater fluid content or different fluid composition (i.e., sink-like ITM) or; 3) large scale advection of fluids to the surface occurred in the pelite, but not in the amphibolite. As discussed above, (1) and (2) are unlikely to explain the difference between pelite and amphibolite before 16 Ma (unless K^{Ar}_d alone varies greatly between pelite and amphibolite). The younger ages of biotite samples within the vein zone suggests that localized advective flow contributes at least somewhat to ^{40}Ar loss from the area. Also, the proximity of the field site to the regional Simplon Fault Zone, which could act as a rapid conduit for Ar, could reduce the effective L for the pelite to only 1 km, relaxing somewhat the severe constraints on D* or V* to keep τ_T in the pelite short.

An alternative hypothesis is that the shorter transmissive timescale of the pelite is accommodated locally (i.e., short L) such that differences in Ar D* (or advective velocity, V*) are not required. Local "sinks" could be present in the form of non-K bearing minerals, such as quartz, which are abundant in the pelite (>50%) but not in the amphibolite (<2%). Such a scenario would negate the requirement of an extremely high Ar D* (or V*) in the pelite because the apparent difference in transmissive timescale, τ_T (L^2/D* or L/V*) could be accounted for entirely by the L term. In the pelite, the diffusive lengthscale, L, for Ar to travel from the source biotite to a local

mineral sink may be millimeters or less. Whereas in the amphibolite, if sink minerals are lacking, the diffusive lengthscale is ~70 cm to reach the sink minerals in the pelite.

To begin to test a local mineral sink hypothesis, information on, 1) the solubility of Ar in the candidate sink mineral; 2) the diffusivity of Ar in the candidate sink mineral and; 3) the equilibrium partition coefficient between the candidate sink mineral, the ITM, and the ^{40}Ar source minerals is needed. An effective sink mineral would have to be open diffusively, sufficiently abundant, and would have to partition Ar at least as strongly as the ^{40}Ar source mineral. Quartz has been little analyzed for Ar but reports of excess ^{40}Ar in quartz suggest that at least some ^{40}Ar may be taken up by that mineral (e.g., Everndon, 1999; Vance et al., 1998). Existing laboratory data (e.g., Roselieb et al., 1997) suggest Ar is highly incompatible in quartz, but more recent data (Watson & Cherniak, 2001) suggest that Ar is in fact highly soluble in quartz. While Ar contained in quartz may actually be present in nano- or microfluid inclusions (e.g., Kelley et al. 1986), this could still make quartz an effective sink for Ar. Furthermore, Ar diffusivities in quartz measured by Watson and Cherniak (2001) appear to be just high enough that quartz may remain open to Ar uptake or release over a wide temperature range (i.e., very low activation energy), even well below that of biotite closure. This means that natural quartz grains analyzed today that may once have been full of ^{40}Ar, could have lost some or all of it at low temperatures after ^{40}Ar source minerals (i.e., biotite) closed. Thus, further laboratory study is required to evaluate quartz, or any mineral, as a potential Ar sink.

This study cannot provide a unique explanation for how the pelite, and apparently any part of the crust where excess ^{40}Ar is absent, maintains an adequately short τ_T with respect to Ar. But it does provide a mechanistic explanation for those portions of the crust that do contain excess Ar (i.e., the amphibolite at site SP5), and, it challenges geochronologists and geochemists to seek more information on the behavior of Ar in the bulk of the crust, where it appears to be less well understood than would be desired.

6. SUMMARY

Detailed spatial sampling of biotites about a lithologic contact between amphibolite and metapelite reveal a significant difference in calculated ^{40}Ar/^{39}Ar ages between pelite and amphibolite biotites. These variations cannot be explained by the effects of grain size, composition, cooling rate, or contamination. A conceptual model hypothesis is introduced in which the presence (or absence) of excess Ar depends on a bulk system property, the transmissive timescales, τ_T, for Ar. Many lithologies (e.g., the pelite or "vein zone") with short τ_T, have no excess Ar, whereas other lithologies (e.g., the amphibolite) with longer τ_T trap within them an amount of locally derived excess ^{40}Ar proportional to τ_T. The data indicate that ambient ^{40}Ar concentrations in the ITM (i.e., ^{40}Ar partial pressures) in the system also varied significantly over centimeter to meter lengthscales. Numerical modeling suggests that the effective steady state diffusivity of Ar in the biotite-amphibolite is $2.2 \pm 1.0 \times 10^{-8}$ m^2/yr and that it must change rapidly at 15.5 ± 1.0 Ma to a new value of less than or equal to 1.0×10^{-11} m^2/yr. The drop in D_{eff} at 15.5 ± 1.0 Ma is likely mechanistically linked to coincident rheological and structural changes in the system and the onset of rapid exhumation.

Our results show that characterization of the argon closure age for biotite in a given system should not rest on a single sample, as otherwise irresolvable differences in "age" between samples within the same outcrop may exist. To sample appropriately so as to achieve geologically meaningful ages, geochronologists must consider the bulk properties of the whole rock, in particular the effective bulk diffusivity of Ar, and the geometry of the system, which together define the transmissive timescale, τ_T. This characteristic bulk rock property (τ_T) is as important as individual mineral properties in the interpretation of ^{40}Ar/^{39}Ar data.

Acknowledgments—We wish to thank Marty Grove, Simon Kelley and Tim Wawrzyniec for their thorough reviews and subsequent fruitful discussions. We thank Mark Harrison for editorial handling and valuable comments on the manuscript. We thank Tim Becker and Kyoungwon Min for their significant help and guidance in ^{40}Ar/^{39}Ar analysis and data reduction. We thank Jane Selverstone and Tim Wawrzyniec for assistance in locating the field site. Funding from NSF grant EAR-9805218 to DJD and from a Berkeley Geochronology Center Fellowship to EFB is gratefully acknowledged.

Associate editor: T. M. Harrison

REFERENCES

Axen, G. J., Selverstone, J. and Wawrzyniec, T. (2001) High-temperature embrittlement of extensional Alpine mylonite zones in the midcrustal ductile-brittle transition. *J. Geophys. Res.* **106,** 4337–4348.

Baxter E. F. (2000) Field Measurement and Implications of Reaction Rates and Chemical Diffusivities in Regional Metamorphic Systems. Unpublished Ph.D. Thesis, University of California, Berkeley.

Baxter E. F. and DePaolo D. J. (2000) Field measurement of slow metamorphic reaction rates at temperatures of 500 to 600 C. *Science.* **288,** 1411–1414.

Bearth P. (1972) Simplon Sheet. *Geologisher Atlas der Schweiz* **1,** 25000. 61.

Berman R.G. (1991) Thermobarometry using multi-equilibria calculations: a new technique, with petrological applications. *Can. Mineral.* **29,** 833–855.

Brady, J. B. (1983) Intergranular diffusion in metamorphic rocks. *Am. J. Sci.* **283A,** 181–200.

Brooker, R. A., Wartho, J-A., Carroll, M. R., Kelley, S. P. and Draper, D. S. (1998) Preliminary UVLAMP determinations of argon partition coefficients for olivine and clinopyroxene grown from silicate melts. *Chem. Geol.* **147,** 185–200.

Burnard P. G., Hu R., Turner G., and Bi X. W. (1999) Mantle, crustal and atmospheric noble gases in Ailaoshan Gold deposits, Yunnan Province, China. *Geochim. Cosmochim. Acta.* **63,** 1595–1604.

Cherniak, D. J. and Watson, E. B. (1994) A study of strontium diffusion in plagioclase using Rutherford backscattering spectroscopy. *Geochim. Cosmochim. Acta.* **58,** 5179–5190.

Crank J. (1975) The Mathematics of Diffusion, 2nd edition. Clarendon Press, Oxford.

Cumbest R. J., Johnson E. L., and Onstott, T. C. (1994) Argon composition of metamorphic fluids: Implications for ^{40}Ar/^{39}Ar geochronology. *Geol. Soc. Am. Bull.* **106,** 942–951.

Dallmeyer R. D. and Rivers, T. (1983) Recognition of extraneous argon components through incremental-release ^{40}Ar/^{39}Ar analysis of biotite and hornblende across the Grenvillian metamorphic gradient in southwestern Labrador. *Geochim. Cosmochim. Acta.* **47,** 413–428.

Dalrymple G. B. and Moore J. G. (1968) Argon-40: Excess in submarine pillow basalts from Kilauea Volcano, Hawaii. *Science.* **161,** 1132–1135.

DePaolo D. J. and Getty S. R. (1996) Models of isotope exchange in

reactive fluid-rock systems: Implications for geochronology in metamorphic systems. *Geochim. Cosmochim. Acta.* **60,** 3933–3947.
Deutsch A. and Steiger R. H. (1985) Hornblende K-Ar ages and the climax of Tertiary metamorphism in the Lepontine Alps (south-central Switzerland): an old problem reassessed. *Earth Planet. Sci. Lett.* **72,** 175–189.
Dodson M. H. (1973) Closure temperature in cooling geochronological and petrological systems. *Contrib. Mineral. Petrol.* **40,** 259–274.
Evernden J. F. (1999) Early developments (1952–1965) in K-Ar geochronology at Berkeley. *Geological Society of America, Cordilleran Section, Abstracts with Programs* **31,** A-53.
Farver, J. R. and Yund, R. A. (1995) Grain boundary diffusion of oxygen, potassium and calcium in natural and hot-pressed feldspar aggregates. *Contrib. Mineral. Petrol.* **118,** 340–355.
Fleck R. J., Sutter J. F., and Elliot D. H. (1977) Interpretation of discordant $^{40}Ar/^{39}Ar$ age-spectra of Mesozoic tholeiites from Antarctica. *Geochim. Cosmochim. Acta.* **41,** 15–32.
Foland K. A. (1979) Limited mobility of argon in a metamorphic terrain. *Geochim. Cosmochim. Acta.* **43,** 793–801.
Foland K. A. (1983) $^{40}Ar/^{39}Ar$ incremental heating plateaus for biotites with excess argon. *Isotope Geosci.* **1,** 3–21.
Giletti B. J. (1974) Studies of diffusion I: argon in phlogopite mica. In *Geochemical Transport and Kinetics* (eds. A. W. Hoffman, B. J. Giletti, H. S. Yoder, and R. A. Yund.) vol. 634, pp. 107–115. Carnegie Institute of Washington Publication.
Goodwin L. B. and Renne P. R. (1991) Effects of progressive mylonitization on grain size and Ar retention of biotites in the Santa Rosa Mylonite Zone, California, and thermochronologic implications. *Contrib. Mineral. Petrol.* **108,** 283–297.
Grasemann, B. and Mancktelow, N. S. (1993) Two-dimensional thermal modeling of normal faulting: the Simplon Fault Zone, Central Alps, Switzerland. *Tectonophysics.* **225,** 155–165.
Grove M. (1993) Thermal histories of southern California basement terranes. Ph.D. dissertation, University of California, Los Angeles.
Grove M. and Harrison T. M. (1996) $^{40}Ar^*$ diffusion in Fe-rich phlogopite. *Am. Mineral.* **81,** 940–951.
Hames, W. E. and Bowring, S. A. (1994) An empirical evaluation of the argon diffusion geometry in muscovite. *Earth Planet. Sci. Lett.* **124,** 161–167.
Harrison T. M. (1981) Diffusion of ^{40}Ar in hornblende. *Contrib. Mineral. Petrol.* **78,** 324–331.
Harrison, T. M. and McDougall, I. (1981) Excess ^{40}Ar in metamorphic rocks from Broken Hill, New South Wales: Implications of $^{40}Ar/^{39}Ar$ age spectra and the thermal history of the region. *Earth Planet. Sci. Lett.* **55,** 123–149.
Harrison T. M., Duncan I., and McDougall I. (1985) Diffusion of ^{40}Ar in biotite: temperature, pressure and compositional effects. *Geochim. Cosmochim. Acta.* **49,** 2461–2468.
Harrison T. M., Heizler M. T., and Lovera O. M., Chen, W., and Grove, M. (1994) A chlorine disinfectant for excess argon released from K-feldspar during step heating. *Earth Planet. Sci. Lett.* **123,** 95–104.
Hess J. C., Lippolt H. J., Gurbanov A. G. and Michalski I. (1993) The cooling history of the late Pliocene Eldzhurtinskiy granite (Caucasus, Russia) and the thermochronological potential of grain-size/age relationships. *Earth Planet. Sci. Lett.* **117,** 393–406.
Hodges K. V., Hames W. E. and Bowring S. A. (1994) 40Ar/39Ar age gradients I nmicas from a high-temperature-low-pressure metamorphic terrain: evidence for very slow cooling and implications for the interpretation of age spectra. *Geol.* **22,** 55–58.
Hodges K. V. and Bowring S. A. (1995) $^{40}Ar/^{39}Ar$ thermochronology of isotopically zoned micas: insights from the southwestern USA Proterozoic orogen. *Geochim. Cosmochim. Acta.* **59,** 3205–3220.
Hyodo H. and York D. (1993) The discovery and significance of a fossilized radiogenic agon wave (argonami) in the Earth's crust. *Geophys. Res. Lett.* **20,** 61–64.
Johnson T. M. and DePaolo D. J. (1994) Interpretation of isotopic data in groundwater systems: Model development and application to Sr isotope data from Yucca Mountain. *Water Res. Res.* **30,** 1571–1587.
Kaneoka I. (1974) Investigation of excess argon in ultramafic rocks from the Kola Peninsula by the $^{40}Ar/^{39}Ar$ method. *Earth Planet. Sci. Lett.* **22,** 145–156.
Kelley S. P. and Wartho J-A. (2000) Rapid kimberlite ascent and the significance of Ar-Ar ages in xenolith phlogopites. *Science.* **289,** 609–611.
Kelley, S., Turner, G., Butterfield, A. W. and Shepherd, T. J. (1986) The source and significance of argon isotopes in fluid inclusions from areas of mineralization. *Earth Planet. Sci. Lett.* **79,** 303–318.
Lanphere M. A. and Dalrymple G. B. (1971) A test of the $^{40}Ar/^{39}Ar$ age spectrum technique on some terrestrial materials. *Earth Planet. Sci. Lett.* **12,** 359–372.
Lanphere M. A. and Dalrymple G. B. (1976) Identification of excess ^{40}Ar by the $^{40}Ar/^{39}Ar$ age spectrum technique. *Earth Planet. Sci. Lett.* **32,** 241–243.
Lovering J. F. and Richards J. R. (1964) Potassium-argon age study of possible lower crust and upper-mantle inclusions in deep-seated intrusions. *J. Geophys. Res.* **69,** 4895–4901.
Maluski H., Monie P., Kienast J. R., and Rahmani A. (1990) Location of extraneous argon in granulite-facies minerals: a paired microprobe-laser probe $^{40}Ar/^{39}Ar$ analysis. *Chem. Geol.* **80,** 193–217.
Mancktelow N. S. (1992) Neogene lateral extension during convergence in the Central Alps: Evidence from interrelated faulting and backfolding around the Simplonpass (Switzerland). *Tectonophys.* **215,** 295–317.
McDougall I. and Green D. H. (1964) Excess radiogenic argon in pyroxenes and isotopic ages on minerals from Norwegian eclogites. *Norsk Geol. Tidsskrift.* **44,** 183–196.
McDougall I. and Harrison T. M. (1999) Geochronology and Thermochonology by the $^{40}Ar/^{39}Ar$ Method. Oxford University Press, New York.
Onstott, T. C., Phillips, D. and Pringle-Goodell, L. (1991) Laser microprobe measurement of chlorine and argon zonation in biotite. *Chem. Geol.* **90,** 145–168.
Pankhurst R. J., Moorbath S., Rex D. C., and Turner G. (1973) Mineral age patterns in ca. 3700 my old rocks from West Greenland. *Earth Planet. Sci. Lett.* **8,** 37–62.
Phillips D. and Onstott T. C. (1988) Argon isotope zoning in mantle phlogopite. *Geol.* **16,** 542–546.
Pickles C. S., Kelley S. P., Reddy S. M., and Wheeler J. (1997) Determinations of high spatial resolution argon isotope variations in metamorphic biotites. *Geochim. Cosmochim. Acta.* **61,** 3809–3833.
Reddy S. M., Kelley S. P., and Wheeler J. (1996) A $^{40}Ar/^{39}Ar$ laser probe study of micas from the Sesia Zone, Italian Alps: implications for metamorphic and deformation histories. *J. Meta. Geol.* **14,** 493–508.
Renne P. R. (1995) Excess ^{40}Ar in biotite and hornblende from the Noril'sk 1 intrusion, Siberia: implications for the age of the Siberian Traps. *Earth Planet. Sci. Lett.* **131,** 165–176.
Renne P. R. (2000) $^{40}Ar/^{39}$ Ar age of plagioclase from Acapulco metorite and the problem of systematic errors in cosmochronology. *Earth Planet. Sci. Lett.* **175,** 13–26.
Renne P. R., Swisher C. C., Deino A. L., Karner D. B., Owens T. L., and DePaolo D. J. (1998) Intercalibration of standards, absolute ages and uncertainties in $^{40}Ar/^{39}Ar$ dating. *Chem. Geol.* **145,** 117–152.
Richards J. R. and Pidgeon R. T. (1963) Some age measurements on micas from Broken Hill, Australia. *Geol. Soc. Aus. J.* **10,** 243–260.
Richter F. M. and DePaolo D. J. (1987) Numerical models for diagenesis and the Neogene Sr isotopic evolution of seawater from DSDP Site 590B. *Earth Planet. Sci. Lett.* **83,** 27–38.
Roddick J. C., Cliff R. A., and Rex D. C. (1980) The evolution of excess argon in alpine biotites—a $^{40}Ar/^{39}Ar$ analysis. *Earth Planet. Sci. Lett.* **48,** 185–208.
Roselieb K., Blanc P., Buttner H., Jambon A., Rammensee W., Rosenhauer M., Vielzeuf D., and Walter H. (1997) Experimental study of argon sorption in quartz: Evidence for argon incompatibility. *Geochim. Cosmochim. Acta.* **61,** 533–542.
Ruffet G., Feraud G., Balevre M., and Kienast J-R. (1995) Plateau ages and excess argon in phengites: an ^{40}Ar-^{39}Ar laser probe study of Alpine micas (Sesia Zone, Western Alps, northern Italy). *Chem. Geol.* **121,** 327–343.
Scaillet S. (1996) Excess ^{40}Ar transport scale and mechanism in high-pressure phengites: a case study from an eclogitized metabasite of the Dora-Maira nappe, western Alps. *Geochim. Cosmichim. Acta.* **60,** 1075–1090.
Smith P. E., York D., Easton R. M., Ozdemir O., and Layer P. W. (1994) A laser ^{40}Ar-^{39}Ar study of minerals across the Grenville

Front: investigation of reproducible excess Ar patterns. *Can. J. Earth Sci.* **31,** 808–817.
Steck A. and Hunziker J. (1994) The Tertiary structural and thermal evolution of the Central Alps—compressional and extensional structures in an orogenic belt. *Tectonophys.* **238,** 229–254.
Vance D. and O'Nions R. K. (1992) Prograde and retrograde thermal histories from the central Swiss Alps. *Earth Planet. Sci. Lett.* **114,** 113–129.
Vance, D., Ayres, M., Kelley, S. and Harris, N. (1998) The thermal response of a metamorphic belt to extension: constraints from laser Ar data on metamorphic micas. *Earth Planet. Sci. Lett.* **162,** 153–164.
Walther J. V. and Wood B. J. (1986) Mineral Fluid Reaction Rates. In *Fluid-Rock Interactions during Metamorphism* (eds. J. V. Walther and B. J. Wood) pp. 194–212. New York, Springer-Verlag.
Watson, E. B. and Cherniak, D. J. (2001) Lattice diffusion and solubility of argon in quartz. In *Eleventh Ann. V.M. Goldschmidt Conference*, Abstract #3279. LPI Contribution No. 1088, Lunar Planet. Inst., Houston (CD-ROM).
Wawrzyniec T., Selverstone J., and Axen G.J. (1999) Correlations between fluid composition and deep-seated structural style in the footwall of the Simplon low-angle normal fault, Switzerland. *Geol.* **27,** 715–718.
Wawrzyniec, T. F., Selverstone, J. and Axen, G. J. (in press) Styles of Footwall Uplift along the Simplon and Brenner Normal Fault Systems, Central and Eastern Alps. *Tectonics* **20,** 748–770.
Zartman R. E., Brock M. R., Heyl A. V., and Thomas H. H. (1967) K-Ar and Rb-Sr ages of some alkalic intrusive rocks from the eastern United States. *Am. J. Sci.* **265,** 848–870.

APPENDIX A

Derivation of Eqations (2) and (3)

These equations, as shown in the text, are similar in form to those derived by Richter and DePaolo (1987). The major difference is in Eqn. 3 and the similar term in Eqn. 2 accounting for the contribution from the solid. To derive this term, begin by considering the flux of moles of ^{40}Ar from the biotite into the fluid, $F^{fluid}_{40_{Ar}}$ within a single element of volume $(dx)^3$. Note that $F^{fluid}_{40_{Ar}}$ is equal and opposite to the flux into the biotite, $F^{solid}_{40_{Ar}}$. This flux (neglecting radiogenic production for the time being) may be written: $-F^{fluid}_{40_{Ar}} = F^{solid}_{40_{Ar}}$ = total ^{40}Ar in biotite at (t) $[^{40}Ar^{t}_{solid}]$ − total ^{40}Ar in biotite at (t−δt) $[^{40}Ar^{t-\delta t}_{solid}]$ because there is no where else for the ^{40}Ar produced in the biotite to go but out into the ITM fluid. Knowing the radial Cs profile in the biotite disk (see Figure A1) from Eqn. 4, we can compute the total amount (in moles) of ^{40}Ar in the biotite at each timestep by summation of i cylindrical shells of width δr and the central cylinder (i=0) of radius $\frac{\delta r}{2}$ as follows:

$$^{40}Ar^{t}_{solid} = C^{t}_{s(0)} \cdot \frac{\pi\rho_s h(\delta r)^2}{4} + \sum_{i=1}^{i_{\max}} C^{t}_{s(i)} \cdot 2\pi i\rho_s h(\delta r)^2 \quad \text{(A1)}$$

and similarly for $[^{40}Ar^{t-\delta t}_{solid}]$. "h" is the effective height of the biotite disk accounting for the mode of biotite:

$$h = \frac{M\%(dx)^3}{\pi a^2} \quad \text{(A2)}$$

Thus,

$$-F^{fluid}_{40_{Ar}} = F^{solid}_{40_{Ar}} = (C^{t}_{s(0)} - C^{t-\delta t}_{s(0)}) \cdot \frac{\pi\rho_s h(\delta r)^2}{4} + \sum_{i=1}^{i_{\max}} (C^{t}_{s(i)} - C^{t-\delta t}_{s(i)}) \cdot 2\pi i\rho_s h(\delta r)^2 \quad \text{(A3)}$$

To express this flux as a change in *concentration* (moles/g) of ^{40}Ar in the fluid (δC_f), we need to scale as follows:

$$\delta C_f = \frac{moles_{40_{Ar}}}{gram_{fluid}} = \frac{F^{fluid}_{40_{Ar}}}{\phi\rho_f (dx)^3} \quad \text{(A4)}$$

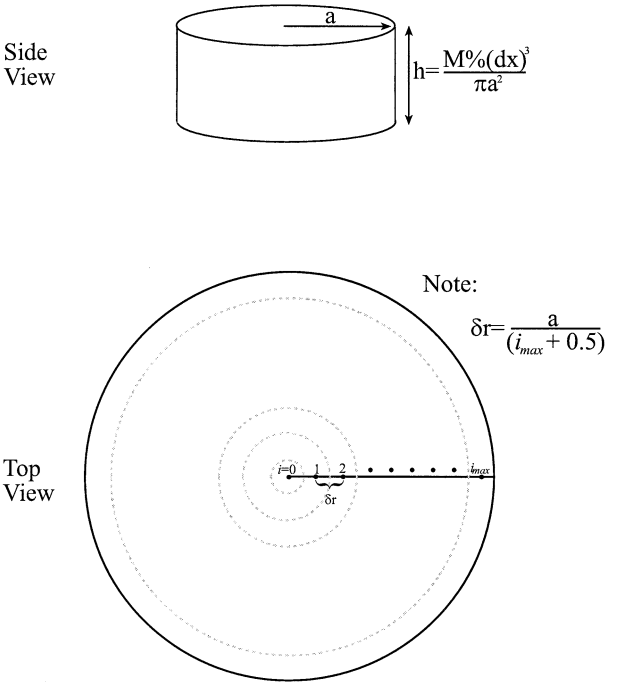

Fig A1. Sketch of numerical approximations in a biotite grain. The height of the biotite is set to account for the variable mode at each point in the system as shown. "i" is the radial index for numerical calculation of the concentration profile in each biotite disc. All diffusion out of the grain is radial. Diffusion parallel to the c-axis is negligible (Onstott et al., 1991; Hames and Bowring, 1994).

Making these substitutions and eliminating like terms finally yields:

$$-\delta C_f = \frac{M(\delta r)^2}{4a^2} \cdot (C^{t}_{s(0)} - C^{t-\delta t}_{s(0)}) + \frac{2M(\delta r)^2}{a^2} \cdot \sum_{i=1}^{i_{\max}} i\,(C^{t}_{s(i)} - C^{t-\delta t}_{s(i)}) \quad \text{(A5)}$$

and, similarly dividing by the density and volume of each shell,

$$\delta C_s = \frac{(\delta r)^2}{4a^2} \cdot (C^{t}_{s(0)} - C^{t-\delta t}_{s(0)}) + \frac{2(\delta r)^2}{a^2} \cdot \sum_{i=1}^{i_{\max}} i(C^{t}_{s(i)} - C^{t-\delta t}_{s(i)}) \quad \text{(A6)}$$

The next step is to expand out the summations for an arbitrary choice of δr and i_{max}, where, given the geometry of the cylindrical numerics,

$$\delta r = \frac{a}{(i_{\max} + 0.5)} \quad \text{(A7)}$$

Following the approach of Crank (1975), the concentration change term inside the summation sign may be approximated numerically by:

$$(C^{t}_{s(i)} - C^{t-\delta t}_{s(i)}) = \frac{D_s}{2i(\delta r)^2}((2i+1)C_{s(i+1)} - 4iC_{s(i)} + (2i-1)C_{s(i-1)})\delta t \quad \text{(A8)}$$

for i=1 to (i_{max}−1) and,

$$(C^{t}_{s(0)} - C^{t-\delta t}_{s(0)}) = \frac{4D_s}{(\delta r)^2}(C_{s(1)} - C_{s(0)})\delta t \quad \text{(A9)}$$

and,

$$(C^{t}_{s(i_{\max})} - C^{t-\delta t}_{s(i_{\max})}) = \frac{D_s}{2i_{\max}(\delta r)^2}\left((2i_{\max}+1)K_dC_f - 4i_{\max}C_{s(i)} + (2i_{\max}-1)C_{s(i-1)}\right)\delta t \quad \text{(A10)}$$

After expanding out terms we find

$$\delta C_{s(\text{ave})} = \frac{2D_s}{a}\cdot\frac{(K_dC_f - C_{s(i_{\max})})}{\delta r}\,\delta t \quad \text{(A11)}$$

and,

$$-\delta C_f = -M\delta C_{s(\text{ave})} = \frac{2MD_s}{a}\cdot\frac{(K_dC_f - C_{s(i_{\max})})}{\delta r}\,\delta t \quad \text{(A12)}$$

Finally, adding in the term in the fluid mediated long-scale diffusion and the term for radiogenic production of ^{40}Ar in the solid, we arrive at the final forms of Eqn. 2 and (3) in the text.